

Towards a sharp, structure preserving two-velocity model for two-phase flow: transport of mass and momentum

Ronald A. Remmerswaal, Arthur E.P. Veldman

*Bernoulli Institute, University of Groningen
PO Box 407, 9700 AK Groningen, The Netherlands*

Abstract

The numerical modelling of convection dominated high density ratio two-phase flow poses several challenges, amongst which is resolving the relatively thin shear layer at the interface. To this end we propose a sharp discretisation of the two-velocity model of the two-phase Navier–Stokes equations. This results in the ability to model the shear layer, rather than resolving it, by allowing for a velocity discontinuity in the direction(s) tangential to the interface.

In this paper we focus our attention on the transport of mass and momentum in the presence of such a velocity discontinuity. We propose a generalisation of the dimensionally unsplit geometric volume of fluid (VOF) method for the advection of the interface in the two-velocity formulation. Sufficient conditions on the construction of donating regions are derived that ensure boundedness of the volume fraction for dimensionally unsplit advection methods. We propose to interpolate the mass fluxes resulting from the dimensionally unsplit geometric VOF method for the advection of the staggered momentum field, resulting in semi-discrete energy conservation. Division of the momentum by the respective mass, to obtain the velocity, is not always well-defined for nearly empty control volumes and therefore care is taken in the construction of the momentum flux interpolant: our proposed flux interpolant guarantees that this division is always well-defined without being unnecessarily dissipative.

Besides the newly proposed two-velocity model we also detail our exactly conservative (mass per phase and total linear momentum) implementation of the one-velocity formulation of the two-phase Navier–Stokes equations, which will be used for comparison.

The discretisation methods are validated using classical time-reversible flow fields, where in this paper the advection is uncoupled from the Navier–Stokes solver, which will be developed in a later paper.

Keywords: two-phase flow, volume of fluid, unresolved shear layer, velocity discontinuity

1. Introduction

The numerical simulation of two-phase flow is of great interest to engineering problems (e.g. liquid sloshing), as well as to fundamental research into fluid flow (e.g. to study the physics of liquid impacts). Discretisation methods used for the transport of mass and momentum play a particularly crucial role, as an erroneous approximation quickly leads to an unphysical exchange of momentum between the phases. For convection dominated high density ratio two-phase flow in particular, it is known that momentum should be conserved [1, 7, 25, 30] while it is transported, for obtaining a robust and accurate model.

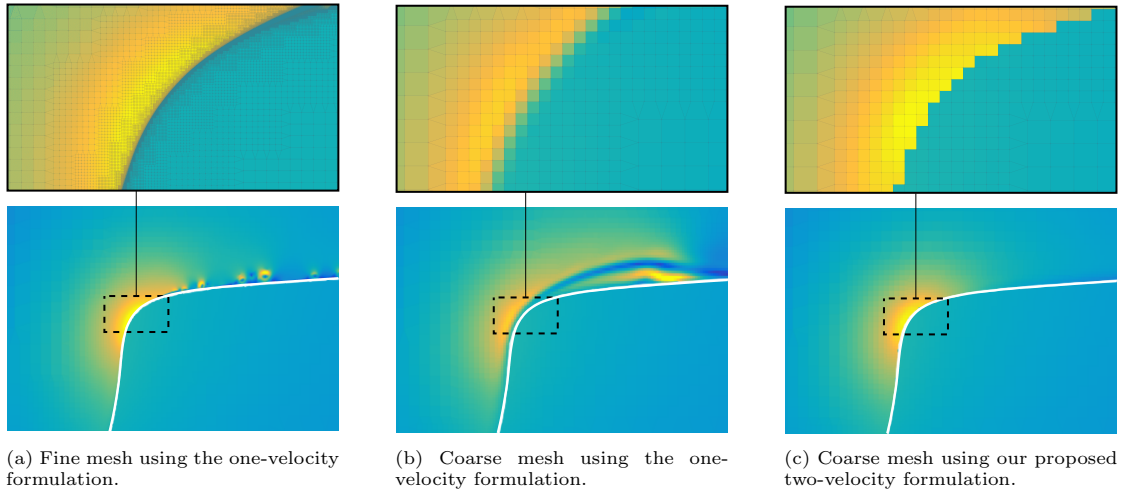


Figure 1: Example simulation of the large gas-pocket impact as defined by Etienne et al. [10] at scale 1 : 5 (thus resulting in a $\lambda = 4\text{m}$ long wave) and $t/T_g \approx 0.45$ (where $T_g = 2\pi/\sqrt{gk}$). We show the velocity magnitude, clipped to $|\mathbf{u}|_2 \in [0, 8]$, at the wave crest and compare three different approximations. The ‘fine’ mesh yields a resolved shear layer with an interface resolution of $h \approx 0.1\text{mm}$ whereas the ‘coarse’ mesh refers to $h \approx 3.1\text{mm}$ (32 times larger). Note that the colouring is determined per control volume (depending on whether the control volume centroid lies in the liquid or gas phase), and therefore the visible ‘staircase’ approximation of the interface is entirely due to postprocessing.

The aforementioned references use methods based on the one-velocity formulation of the two-phase NSE, wherein the velocity field is assumed to be continuous at the interface

$$[[\mathbf{u}]] = 0. \quad (1)$$

Here the jump in a quantity is defined as the difference between the gas and liquid value

$$[[\varphi]] := \varphi^g - \varphi^l, \quad \{\{\varphi\}\} := \varphi^g + \varphi^l,$$

where we have introduced a complimentary notation for the sum over the phases. This one-velocity formulation results in a single set of equations defined in the entire computational domain Ω , where the fluid properties (i.e. the density and dynamic viscosity) change when going from the liquid to the gas domain. The simulation of convection dominated high density ratio two-phase flow, however, can be quite challenging due to the formation of a viscous boundary layer at the interface, which we will refer to as a ‘shear layer’. In figs. 1a and 1b we show two approximate solutions according to the one-velocity formulation on a fine as well as relatively coarse (but still fine enough to resolve the interface) mesh. Perhaps unsurprisingly we find, due to the assumption of velocity continuity at the interface, that the thickness of the shear layer is determined by the mesh resolution until it is entirely resolved. This implies that the dynamics in the lighter gas phase are incorrectly approximated until the shear layer is resolved, which raises the question of whether such a shear layer can successfully be modelled. Thus resulting in a numerical model for two-phase flow in which the shear layer need not be resolved, from which it follows that the resolution requirements become independent of viscous effects.

We will propose a numerical model for incompressible two-phase flow that is based on a two-velocity formulation of the two-phase NSE [11, 27, 31]. This means that each phase gets its own momentum (and thus velocity) field, as well as the corresponding equation which governs its conservation. Rather than imposing continuity of the velocity field, we now merely impose

that the interface normal component of the velocity is continuous (i.e., there is no phase change)

$$[[u_\eta]] = 0, \quad (2)$$

where $\boldsymbol{\eta}$ denotes the interface normal (pointing into the gas phase), and the interface normal component of the velocity is denoted by $u_\eta = \boldsymbol{\eta} \cdot \mathbf{u}$. The resulting numerical model therefore aims at replacing the unresolved shear layer by a velocity discontinuity in the direction(s) tangential to the interface, as shown in fig. 1c.

Several multi-equation models for two-phase flow can be found in the literature, resulting in at most two mass conservation equations, two momentum conservation equations, two energy equations and an equation that governs the advection of the interface. In Saurel and Abgrall [31] a hyperbolic seven equation model (2-2-2-1) is considered for the simulation of two-phase compressible flow. The energy equations are omitted in Preisig and Zimmermann [27], who therefore consider a five equation model (2-2-0-1), and in Favrie et al. [11] a six equation model (2-1-2-1) is considered where a momentum equation for the mixture is considered.

For incompressible two-phase flow not much can be found in the literature regarding multi-equation models (in particular two-velocity models). Note that for incompressible flow the mass conservation equations are implied by the equation that governs the advection of the interface, together with a suitable incompressibility constraint (which we will count as a mass conservation equation). In Desjardins and Moureau [6] and Vukčević et al. [39] two separate equations are used for the transport of momentum, but after each time step the velocity jump is removed in the pressure Poisson problem by imposing eq. (1). In our terminology this constitutes as a one-velocity model (1-1-0-1). Our proposed two-velocity model is a sharp four equation model (1-2-0-1) wherein the velocity is permitted to be discontinuous according to eq. (2).

The numerical modelling of such a two-velocity formulation poses many challenges, but we will focus our attention on the following three.

Challenges 1 (Two-velocity formulation). *In the presence of a velocity discontinuity, how to...*

- 1) *transport mass and momentum*
- 2) *impose continuity of the interface normal component of velocity*
- 3) *ensure that the viscous one-velocity solution is obtained under mesh refinement*

For now we will consider challenge 1.1, which means that the two fluids are not yet coupled. The coupling of the fluids, via the interface normal component of velocity, as well as viscous diffusion, is considered in a future paper where the entire Navier–Stokes solver will be detailed.

The transport of mass ($\varphi^\pi = 1$) and momentum ($\boldsymbol{\varphi}^\pi = \mathbf{u}^\pi$) is modelled, in conservative integral form, by

$$\int_{\omega^{\pi,(n+1)}} \rho^\pi \varphi^\pi dV - \int_{\omega^{\pi,(n)}} \rho^\pi \varphi^\pi dV + \int_{t^{(n)}}^{t^{(n+1)}} \int_{\partial\omega^\pi(t) \setminus I(t)} \rho^\pi u_n^\pi \varphi^\pi dS dt = 0, \quad (3)$$

which is illustrated in fig. 2, with $\omega = c$. Here ω denotes some fixed in time control volume, $\omega^{\pi,(n)}$ denotes the part of this control volume which is occupied by the π -phase at $t = t^{(n)}$ and $I(t)$ denotes the interface, where $\pi \in \{l, g\}$ denotes the respective phase. Furthermore, u^π denotes the velocity of the π -phase and ρ^π the corresponding (constant) density.

The advection of the phase interface is closely related to the conservation of mass, and more specifically, the conservation of mass is implied (our fluids are assumed incompressible) by the conservation of phase volume. Therefore we focus our attention on geometric volume of fluid

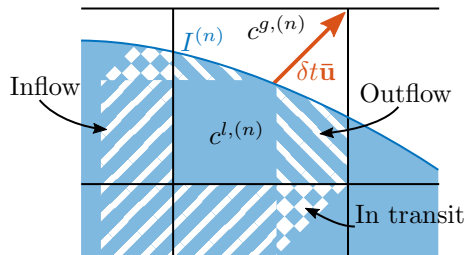


Figure 2: Illustration of eq. (3). A centred control volume c is shown, separated by the interface $I^{(n)}$, resulting in two parts $c^{\pi,(n)}$. The hatched regions correspond to liquid that flows into, through (referred to as ‘in transit’) and out of the control volume c during the time interval $[t^{(n)}, t^{(n+1)}]$. Here the advecting velocity is proportional to $[1, 1]^T$ and shown by the arrow.

(VOF) methods, see e.g. the works of Hirt and Nichols [15], Youngs [41], Rider and Kothe [29], Puckett et al. [28], Rudman [30], Harvie and Fletcher [13], Lopez et al. [22], Weymouth and Yue [40] and Owkes and Desjardins [24]. Amongst those references, we find that only [24] results in a sharp dimensionally unsplit interface advection method which exactly conserves volume, and therefore mass, without the need of using unphysical mass redistribution algorithms, and moreover does not produce any wisps, flotsam and/or jetsam.

Several approaches can be taken in the discretisation of eq. (3) for $\varphi^\pi \neq 1$ (not constant). In Desjardins and Moureau [6] and Desmons and Coquerelle [7] the conservative integral form is first converted into a strong form

$$\partial_t(\rho\varphi)^\pi + \nabla \cdot (\rho\mathbf{u}\varphi)^\pi = 0,$$

where for simplicity in notation we write $(\rho\varphi)^\pi = \rho^\pi\varphi^\pi$. This strong formulation is then discretised using one-sided extrapolation [6] (reminiscent of the ghost fluid method [21]) or using standard methods for hyperbolic problems [7]. Neither of such approaches results in exact conservation of mass and linear momentum combined with a sharp interface representation.

Instead, we follow the approach which was first introduced in Rudman [30], and later adopted by Chenadec and Pitsch [3], Owkes and Desjardins [25], Zuzio et al. [43] and Arrufat et al. [1] for one-velocity formulations. This approach is based on an approximate space-time integration of the space-time integral in eq. (3), and directly results in conservative transport on a collocated variable layout. Our proposed advection method differs in the way this approach is generalised for a staggered momentum field.

Overview

We will first introduce some frequently occurring notation in section 2. In section 3 we will discuss the dimensionally unsplit discretisation of the interface advection equation, for both the one- and two-velocity formulation, and derive sufficient conditions that guarantee boundedness of the volume fraction. As the fluids are considered incompressible, the advection equation of the interface directly yields the centred mass conservation equations. A dimensionally unsplit advection method for the staggered momentum field is proposed and analysed in section 4, and is furthermore compared with methods found in the literature. Results are shown and discussed in section 5 and we conclude with a preliminary discussion in section 6.

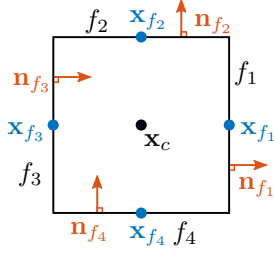


Figure 3: A control volume $c \in \mathcal{C}$ with boundary $\partial c = \bigcup_{f \in \mathcal{F}(c)} f$, where $\mathcal{F}(c) = \{f_1, f_2, f_3, f_4\}$. Here $o_{c,f_1} = o_{c,f_2} = +1$ and $o_{c,f_3} = o_{c,f_4} = -1$.

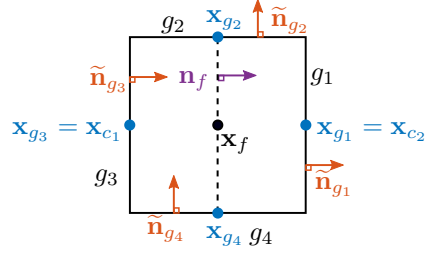


Figure 4: A staggered control volume ω_f based on the extrusion of the face $f \in \mathcal{F}$ (dashed line) to the centroids of the neighbouring control volumes $\mathcal{C}(f) = \{c_1, c_2\}$. The faces of the staggered control volume are given by $\mathcal{G}(\omega_f) = \{g_1, g_2, g_3, g_4\}$.

2. Notation

2.1. Computational mesh

The mesh we use is *locally* rectilinear in the sense that the mesh is an adaptive block-based mesh, where each block is rectilinear. Details on the block-based mesh, as well as modifications of the operators presented here near refinement interfaces, can be found in Van der Plas [35]. Even though we consider a rectilinear mesh, we choose to use a general notation suitable for an arbitrary tessellation of the domain, as presented in Lipnikov et al. [20]. The reason for using this notation is that most of the discretisation methods we propose can in fact be applied to an arbitrary tessellation of the domain.

Rather than using indices i, j, k (which imply the use of a logically rectilinear mesh) to denote some control volume $c_{i,j,k}$ we simply refer to some control volume $c \subset \Omega \subset \mathbb{R}^d$, where $d = 2, 3$ denotes the dimensionality of the domain Ω . The set of all control volumes is denoted by \mathcal{C} . Each control volume c has faces which are denoted by $f \in \mathcal{F}(c)$, where $\mathcal{F}(c)$ is the set of all faces of the control volume c , see also fig. 3. Similarly, the control volumes adjacent to some face f are denoted by the set $\mathcal{C}(f)$. The set of all faces is denoted by \mathcal{F} .

The staggered control volume is defined as the extrusion of the face f to the neighbouring control volume centroids \mathbf{x}_c for $c \in \mathcal{C}(f)$, and is denoted by ω_f , see also fig. 4. The centroid of a face f is denoted by \mathbf{x}_f . The boundary of a staggered control volume consists of faces $g \in \mathcal{G}(\omega_f)$, where \mathcal{G} is the set of all such staggered faces.

2.2. Function spaces and operators

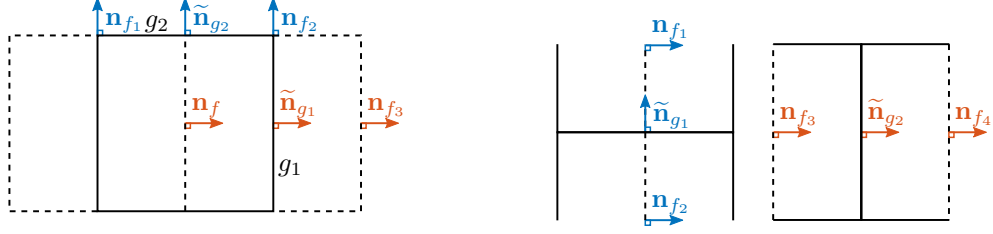
For the centred and staggered control volumes we define corresponding function spaces. The centred functions, such as the pressure $p \in \mathcal{C}^h : \mathcal{C} \rightarrow \mathbb{R}$, are such that the value of p_c approximates the value of p in the centroid of the control volume

$$p_c^{(n)} \approx p(t^{(n)}, \mathbf{x}_c).$$

Similarly, the staggered functions, such as the velocity and momentum, $u \in \mathcal{F}^h : \mathcal{F} \rightarrow \mathbb{R}$ approximate the face-normal component of velocity at the face centroid

$$u_f^{(n)} \approx \mathbf{n}_f \cdot \mathbf{u}(t^{(n)}, \mathbf{x}_f),$$

where \mathbf{n}_f is normal to the face f . The tensor valued functions are defined at the centroids of the faces of the staggered control volumes (denoted by \mathbf{x}_g as shown in fig. 4), that is, $T \in \mathcal{G}^h : \mathcal{G} \rightarrow \mathbb{R}$



(a) Illustration of the set of neighbouring faces $\mathcal{F}(g)$. The set of faces that overlap with g_2 is given by $\mathcal{F}(g_2) = \{f_1, f_2\}$, whereas the set of neighbouring faces with the same face normal direction as g_1 is given by $\mathcal{F}(g_1) = \{f, f_3\}$.

(b) Illustration of the set of neighbouring faces $\mathcal{F}^\omega(g)$. The set of faces whose staggered control volume share g_1 as a boundary is given by $\mathcal{F}^\omega(g_1) = \{f_1, f_2\}$. Similarly, for g_2 this set is given by $\mathcal{F}^\omega(g_2) = \{f_3, f_4\}$.

Figure 5: The solid boundaries correspond to staggered control volumes ω_f , whereas the dashed boundaries correspond to the centred control volumes c .

is defined such that

$$\tilde{o}_{f,g} T_g^{(n)} \approx \mathbf{n}_f \cdot \mathbf{T}(t^{(n)}, \mathbf{x}_g) \cdot \tilde{\mathbf{n}}_g.$$

The divergence operator $\mathfrak{D} : \mathcal{F}^h \rightarrow \mathcal{C}^h$ is defined as a boundary integral divided by the control volume size $|c|$

$$|c|(\mathfrak{D}u)_c := \sum_{f \in \mathcal{F}(c)} |f| o_{c,f} u_f \approx \int_{\partial c} \mathbf{u} \cdot \mathbf{n} dS, \quad (4)$$

where o encodes the local orientation of the face normal \mathbf{n}_f such that $o_{c,f} \mathbf{n}_f$ is pointing out of the centred control volume c and $|f|$ denotes the area (length in 2D) of the face f . See also fig. 3. The gradient $\mathfrak{S} : \mathcal{C}^h \rightarrow \mathcal{F}^h$ is defined as the negative adjoint (w.r.t. the L^2 inner product) of \mathfrak{D} . That is, \mathfrak{S} is defined exactly such that

$$\sum_{c \in \mathcal{C}} |c| p_c (\mathfrak{D}u)_c = - \sum_{f \in \mathcal{F}} |\omega_f| u_f (\mathfrak{S}p)_f, \quad \forall p \in \mathcal{C}^h, u \in \mathcal{F}^h,$$

where we have assumed that the boundary contributions vanish (periodic domain or no-slip/slip boundary conditions). This results in the following definition of the gradient operator

$$(\mathfrak{S}p)_f := -\frac{1}{h_f} \sum_{c \in \mathcal{C}(f)} o_{c,f} p_c \approx \mathbf{n}_f \cdot \nabla p(\mathbf{x}_f), \quad (5)$$

where $h_f := |\omega_f|/|f|$ denotes the face projected distance between the centroids of the neighbouring control volumes of the face f . Furthermore we consider the interpolant $\mathfrak{I} : \mathcal{C}^h \rightarrow \mathcal{F}^h$, which weighs each scalar value by their respective control volume size

$$|\omega_f|(\mathfrak{I}\alpha)_f := \frac{1}{2} \sum_{c \in \mathcal{C}(f)} |c| \alpha_c. \quad (6)$$

This interpolant is consistent because $|\omega_f| = \frac{1}{2} \sum_{c \in \mathcal{C}(f)} |c|$.

For the staggered control volume ω_f we define the staggered divergence operator $\tilde{\mathfrak{D}} : \mathcal{G}^h \rightarrow \mathcal{F}^h$ in terms of a boundary integral over the faces $g \in \mathcal{G}(\omega_f)$ divided by the staggered control volume size $|\omega_f|$

$$|\omega_f|(\tilde{\mathfrak{D}}T)_f := \sum_{g \in \mathcal{G}(\omega_f)} \tilde{o}_{f,g} |g| T_g, \quad (7)$$

where $\tilde{o}_{f,g}$ is such that $\tilde{o}_{f,g}\tilde{\mathbf{n}}_g$ points out of ω_f . The area of the face $g \subset \partial\omega_f$ is defined as

$$|g| := \frac{1}{2} \sum_{f \in \mathcal{F}(g)} |f|,$$

where $\mathcal{F}(g)$ is the set of faces $f \in \mathcal{F}$ neighbouring g with the same face normal direction, as illustrated in fig. 5a. As with the standard divergence and gradient operators $\mathfrak{D}, \mathfrak{S}$ we define staggered gradient operator $\tilde{\mathfrak{S}} : \mathcal{F}^h \rightarrow \mathcal{G}^h$ as the negative adjoint of $\tilde{\mathfrak{D}}$. This results in

$$(\tilde{\mathfrak{S}}u)_g = -\frac{1}{\tilde{h}_g} \sum_{f \in \mathcal{F}^\omega(g)} \tilde{o}_{f,g} u_f,$$

where $\mathcal{F}^\omega(g)$ denotes the set of neighbouring staggered control volumes which have g as part of their boundary, as shown in fig. 5b. The distance \tilde{h}_g is defined such that $\tilde{\mathfrak{S}}$ is exact for linear functions. Finally we denote by $\tilde{\mathfrak{I}} : \mathcal{F}^h \rightarrow \mathcal{G}^h$ the area weighted interpolant for interpolation of staggered fields to tensor valued functions

$$|g|(\tilde{\mathfrak{I}}m)_g := \frac{1}{2} \sum_{f \in \mathcal{F}(g)} (\tilde{\mathbf{n}}_g \cdot \mathbf{n}_f) |f| m_f. \quad (8)$$

A relation between all of the previously introduced operators, which will be important later on, is stated in lemma 1 and proven in Appendix A.

Lemma 1 (Operator connection). *For the previously introduced operators eqs. (4) and (6) to (8) it holds that*

$$\tilde{\mathfrak{D}}\tilde{\mathfrak{I}} = \mathfrak{I}\mathfrak{D}. \quad (9)$$

3. Transport of mass

The equation that governs conservation of the centred mass can be obtained from eq. (3) by letting $\varphi^\pi = 1$ and letting the control volume coincide with a centred control volume $\omega = c$

$$\int_{c^{\pi,(n+1)}} \rho^\pi dV - \int_{c^{\pi,(n)}} \rho^\pi dV + \sum_{f \in \mathcal{F}(c)} \int_{t^{(n)}}^{t^{(n+1)}} \int_{f^\pi(t)} \rho^\pi u^\pi dS dt = 0. \quad (10)$$

Here we moreover replaced the integration over the boundary $\partial c \setminus I(t)$ by a sum of integrals over the π -phase part of the faces, which follows from

$$\partial c^\pi \setminus I(t) = \bigcup_{f \in \mathcal{F}(c)} f^\pi(t).$$

As briefly motivated in the introduction, we will use the geometric VOF method for the advection of the interface. Hence the d -dimensional phase domain $\Omega^\pi \subset \Omega \subset \mathbb{R}^d$, for $\pi \in \{l, g\}$, will implicitly be represented by the volume fraction function $\alpha^\pi \in \mathcal{C}^h$, where the volume fraction α_c^π is defined as the fraction of volume in the control volume c occupied by the π -phase

$$\alpha_c^\pi := \frac{|c^\pi|}{|c|} \in [0, 1].$$

Since the fluids are assumed incompressible we can factor out the constant density ρ^π in eq. (10), resulting in

$$|c|\alpha_c^{\pi,(n+1)} - |c|\alpha_c^{\pi,(n)} + \sum_{f \in \mathcal{F}(c)} \int_{t^{(n)}}^{t^{(n+1)}} \int_{f^\pi(t)} u_n^\pi dS dt = 0. \quad (11)$$

This is a volumetric constraint on the advection of the interface, and in particular, summation of eq. (11) over all control volumes $c \in \mathcal{C}$ shows that the volume of each of the phases should be constant in time (provided an absence of in- or outflow at the boundary). Adding the volumetric constraints for both phases results in (after letting the time step $\delta t = t^{(n+1)} - t^{(n)}$ tend to zero)

$$\int_{\partial c} u_n dS = 0, \quad (12)$$

where the boundary integral contains contributions from the liquid as well as the gas velocity.

Sharp interface approximations of eq. (11) are obtained by a sharp approximation of the space-time integral, which often rely on the geometric intersection of an approximate donating region (DR) [42] with an approximate phase domain representation Ω^π . The geometric VOF method traditionally relies on the piecewise linear approximation of the interface within each interface control volume, i.e.

$$c^l := \{ \mathbf{x} \in c \mid \boldsymbol{\eta}_c \cdot (\mathbf{x} - \mathbf{x}_c) + s(\boldsymbol{\eta}_c; \alpha_c^l) \leq 0 \}, \quad c^g := c \setminus c^l.$$

We choose to approximate the interface normal $\boldsymbol{\eta} \in [\mathcal{C}^h]^d$ by making use of local height-functions (LHFs) [12, 37] when possible, and if this is not possible we resort to the efficient least-squares VOF interface reconstruction algorithm (ELVIRA) [26]. Provided with the interface normal and volume fraction, the shift $s(\boldsymbol{\eta}_c; \alpha_c^l)$ is defined by ensuring that the volume of the reconstructed liquid part coincides with $|c|\alpha_c^l$, which can be achieved using the methods described by Scardovelli and Zaleski [32].

In what follows we will discuss the geometric VOF method for the one-velocity formulation in detail, i.e. we discuss the discretisation of the space-time integral in eq. (11). We will first define some convenient notation for the oriented DR. Then we derive sufficient conditions for the construction of approximate DRs which will ensure that the resulting volume fraction is bounded between zero and one. Subsequently we will consider some DR approximation methods found in the literature in light of these conditions.

Provided with a discretisation of eq. (11), the transport of the centred mass is modelled by denoting the mass per phase as $|c|\alpha_c^{\pi,(n)}\rho^\pi$, whose evolution equation directly follows from the evolution of the volume fraction function $\alpha^{\pi,(n)}$. We will furthermore propose a generalisation of the interface advection method for the two-velocity model.

3.1. The oriented donating region

For the moment we will assume that our velocity field is continuous, as is the case in the one-velocity model. We emphasise this by denoting the velocity by $\bar{\mathbf{u}} \in \mathcal{F}^h$. For the evaluation of the space-time integral in eq. (11) we will use a geometric intersection of a donating region with the phase domain. The DR, which will be denoted by $\bar{\Delta}_f^{(n)}$, is defined as the set of points for which the following equality holds

$$M_0(\bar{\Delta}_f^{(n)} \cap \Omega^{\pi,(n)}) = \int_{t^{(n)}}^{t^{(n+1)}} \int_{f^\pi(t)} u_n^\pi dS dt, \quad (13)$$

where M_0 denotes the signed volume of a set, and will be defined in eq. (14).

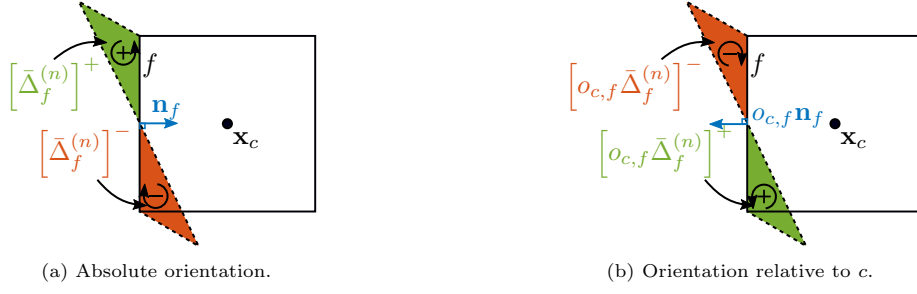


Figure 6: Illustration of an oriented and self-intersecting DR. The positively oriented part consists of the points that flow through the face f in the direction of the face normal, whereas the negatively oriented part consists of points that flow through the face f in the direction opposite to the face normal. When the face normal \mathbf{n}_f is considered we refer to the orientation of the part as the absolute orientation (left), and if the face normal $o_{c,f}\mathbf{n}_f$ is considered, we refer to it as the relative orientation instead (right).

The DR is endowed with an orientation such that a volume flux can be both positively as well as negatively contributing. Note that a DR may self intersect, resulting in a DR which contains a positively as well as a negatively oriented part. The orientation of a part of the DR $\bar{\Delta}_f^{(n)}$ is defined as negative if the face normal \mathbf{n}_f points into it, see also fig. 6a.

Instead of separately having to keep track of each of the parts of the DR per face, we introduce the following notation: an oriented set Δ is defined as a pair of non-oriented sets

$$\Delta = (\Delta^+, \Delta^-), \quad \Delta^\pm \subset \mathbb{R}^d,$$

where Δ^+, Δ^- equals the positively and negatively oriented part respectively. The signed volume is then defined as the difference between the unsigned volumes

$$M_0(\Delta) := |\Delta^+| - |\Delta^-|. \quad (14)$$

Intersection of an oriented set Δ with a non-oriented set A is defined per oriented part

$$\Delta \cap A := (\Delta^+ \cap A, \Delta^- \cap A),$$

and the union, intersection as well as set difference of two oriented sets are defined ‘elementwise’, e.g.

$$\Delta \cap \nabla := (\Delta^+ \cap \nabla^+, \Delta^- \cap \nabla^-).$$

Moreover, we allow the orientation of the parts of an oriented set to be swapped, which we denote as the multiplication by minus one (for two non-oriented sets A, B)

$$-(A, B) := (B, A). \quad (15)$$

We refer to the orientation of $o_{c,f}\bar{\Delta}_f^{(n)}$ (recall that $o_{c,f} = \pm 1$) as the orientation of the DR relative to the control volume c , or simply as the ‘relative orientation’. This is illustrated in fig. 6b. Note that DRs of opposite relative orientation may overlap, resulting in a volume flux that cancels due to the opposite relative orientation, and which corresponds to fluid that merely passes through the control volume c : the fluid is ‘in transit’ while in c (see also fig. 2).

Remark 1 (Definition of the donating region). *Often the DR is defined as the set of points that are fluxed through the face f during the time interval $[t^{(n)}, t^{(n+1)}]$*

$$\bar{\Delta}_f^{(n)} := \{ \Phi_{t^{(n+1)}}^{-\tau} f \mid \tau \in [0, \delta t] \},$$

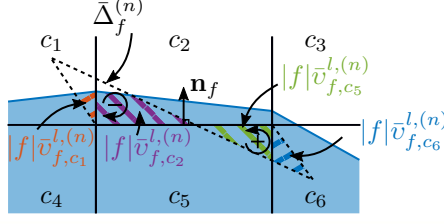


Figure 7: Example of a self-intersecting DR (dashed), intersected with the neighbouring phase domain (shaded), resulting in the partial volume fluxes (hatched regions). The neighbouring control volumes are given by $\mathcal{C}^2(f) = \{c_1, \dots, c_6\}$, and four out of six of the partial volume fluxes are nontrivial.

where the flow map $\Phi_{t_0}^\tau$ is the solution operator of the following initial value problem

$$\frac{d}{dt}\mathbf{x}(t) = \bar{\mathbf{u}}(t, \mathbf{x}(t)), \quad \mathbf{x}(t_0) = \mathbf{x}_0,$$

such that $\Phi_{t_0}^\tau \mathbf{x}_0 = \mathbf{x}(t_0 + \tau)$.

This definition however does not in general satisfy eq. (13), but it is sufficient for our discussion and we will therefore make use of it. For a precise definition we refer to Zhang and Ding [42].

3.2. Geometric VOF for the one-velocity model

Provided with the defining equation (13) of the DR, we can rewrite eq. (11) as follows

$$\frac{\alpha^{\pi,(n+1)} - \alpha^{\pi,(n)}}{\delta t} + \mathfrak{D}\bar{v}^{\pi,(n)} = 0, \quad (16)$$

where the divergence operator \mathfrak{D} is as defined in eq. (4), and the signed volume flux $\bar{v}^{\pi,(n)} \in \mathcal{F}^h$ is given by the intersection volume of the DR with the phase domain

$$\delta t |f| \bar{v}_f^{\pi,(n)} := M_0(\bar{\Delta}_f^{(n)} \cap \Omega^{\pi,(n)}). \quad (17)$$

As the phase domain is approximated piecewise linearly, the volume flux is also computed in a piecewise manner

$$\bar{v}_f^{\pi,(n)} = \sum_{b \in \mathcal{C}} \bar{v}_{f,b}^{\pi,(n)}, \quad (18)$$

where $|f| \bar{v}_{f,b}^{\pi,(n)}$ is the ‘partial volume flux’ and results from the fluid that flows through the face f and comes from the neighbouring control volume b . The partial volume flux is defined as

$$\delta t |f| \bar{v}_{f,b}^{\pi,(n)} := M_0(\bar{\Delta}_f^{(n)} \cap b^{\pi,(n)}), \quad (19)$$

as illustrated in fig. 7. Note that under a suitable CFL constraint the use of the set \mathcal{C} in eq. (18) can be replaced by $\mathcal{C}^2(f)$, which is the set of all control volumes that share at least one node with f (i.e. $2 \times 3^{d-1}$ control volumes for a rectilinear mesh).

For the approximate advection of the interface we will approximate both terms on the right-hand side of eq. (17): the fluid domain is approximated using a piecewise linear reconstruction of the interface, whereas the DR is replaced by a polytopal approximation. In what follows we will discuss types of so called ‘fluxing errors’ that result from poorly approximated DRs, and subsequently we show that the absence of such fluxing errors results in a dimensionally unsplit advection method for which boundedness of the volume fraction can be guaranteed. Moreover we discuss several advection methods from the literature, and check which of the fluxing errors are made.

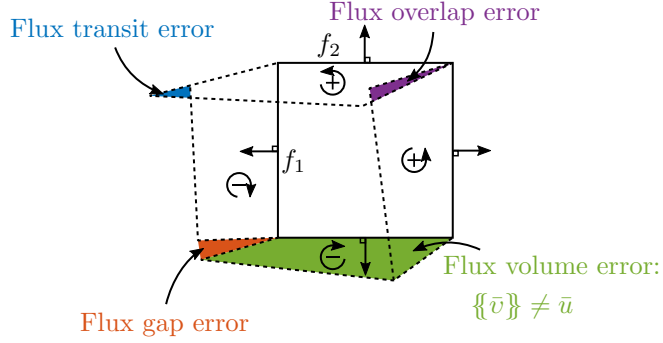


Figure 8: Example of four two-dimensional donating regions (black dashed lines, each defined by four vertices) defined for some control volume c (black solid line) resulting in four fluxing errors: the flux overlap error results from erroneously overlapping (i.e. of same relative orientation) DRs, the flux gap error results from a gap between two neighbouring DRs, and the flux transit error results from two neighbouring DRs with no overlap or gap, but which are defined using a non-matching corner position. Finally, it must be ensured that the volume of the DR matches the total volume flux according to $\delta t |f| \bar{u}_f$, as stated in eq. (23). Note that the orientation shown here is relative to the control volume c .

3.2.1. Fluxing errors in approximate donating regions

When approximating a DR it is important to keep in mind that, besides the approximation errors, boundedness of the resulting volume fraction is of importance. Some approximation errors may result in what we call fluxing errors, which for example lead to a piece of fluid that is fluxed twice during a single time step, potentially resulting in unboundedness of the volume fraction. An absence of fluxing errors does not imply an absence of approximation errors, but we will show that an absence of fluxing errors results in guaranteed boundedness of the volume fraction. This result will be formalised in corollary 1, which to the best of our knowledge is new, and can be used as a guide in the design of approximate DR methods. We will now discuss four different fluxing errors, three of which will turn out to be essential for boundedness, and which are illustrated in fig. 8.

Flux overlap error. Erroneously constructed DRs may result in overlap of two neighbouring DRs with equal relative orientation, as shown by the purple shaded region in fig. 8. This implies that the corresponding fluid (if any) will leave the control volume c twice, therefore potentially resulting in unboundedness of the volume fraction. We refer to this as a flux overlap error, which is defined as

$$\left[o_{c,f} \bar{\Delta}_f^{(n)} \right]^+ \cap \left[o_{c,g} \bar{\Delta}_g^{(n)} \right]^+ \neq \emptyset, \text{ for some } f \neq g \in \mathcal{F}(c), \quad (20)$$

and similarly for the negatively oriented counterpart.

Flux gap error. There may also be a gap between two neighbouring DRs, which implies that the fluid (if any) will erroneously remain inside the neighbouring control volume, potentially resulting in wisps [34], which are tiny fragments of fluid which are erroneously jettisoned from the bulk. See e.g. the red shaded region in fig. 8. Such an error is referred to as flux gap error.

Flux transit error. While overlapping DRs are permissible if they have opposite relative orientation, care should be taken that they do not result in what we refer to as a flux transit error, shown in fig. 8 as the blue shaded region. Here a mismatch in the DR corner position results in fluid that leaves c through f_2 , but does not enter c via f_1 . This can lead to unboundedness

of the volume fraction. A flux transit error (referred to as the existence of ‘nonconforming flux polyhedra’ in Ivey and Moin [16]) is defined as

$$\underbrace{\left[o_{c,f}\bar{\Delta}_f^{(n)}\right]^+}_{\text{leaving}} \setminus \bigcup_{g \in \mathcal{F}(c)} \underbrace{\left[o_{c,g}\bar{\Delta}_g^{(n)}\right]^-}_{\text{entering}} \not\subset c, \text{ for some } f \in \mathcal{F}(c). \quad (21)$$

Flux volume error. Finally, note that if eq. (16) is summed over $\pi = l, g$ we find that

$$\{\!\!\{\alpha}\!\!\}^{(n+1)} - \{\!\!\{\alpha}\!\!\}^{(n)} + \mathfrak{D}\{\!\!\{\bar{v}\}\!\!\}^{(n)} = 0 \implies \mathfrak{D}\{\!\!\{\bar{v}\}\!\!\}^{(n)} = 0, \quad (22)$$

since both phases together fill up a control volume $\{\!\!\{\alpha}\!\!\} = 1$. By definition of the volume flux in eq. (17) we find that the sum of the volume fluxes equals the signed volume of the DR

$$\delta t |f| \{\!\!\{\bar{v}\}\!\!\}_f^{(n)} = M_0(\bar{\Delta}_f^{(n)}).$$

and therefore the volume of the exact DR should equal the exact total volume flux

$$M_0(\bar{\Delta}_f^{(n)}) = \int_{t^{(n)}}^{t^{(n+1)}} \int_f \bar{u}_n \, dS \, dt \approx \delta t |f| \bar{u}_f^{(n)}.$$

Hence we will impose that the volume of the DR should equal the total volume flux [22]

$$M_0(\bar{\Delta}_f^{(n)}) \approx \delta t |f| \bar{u}_f^{(n)}, \quad (23)$$

such that we find that eq. (22) holds automatically by the incompressibility constraint $\mathfrak{D}\bar{u}^{(n)} = 0$. Note that eq. (23) approximately holds for exact DRs, but we impose it to hold exactly for approximate DRs. The fourth error that we consider is the flux volume error, which occurs when the signed volume of the DR (as defined in eq. (14)) does not match the total volume flux $\delta t |f| \bar{u}_f^{(n)}$. This can be expressed as

$$\{\!\!\{\bar{v}\}\!\!\}_f^{(n)} \neq \bar{u}_f^{(n)}.$$

Imposing that all types of fluxing errors are absent does not leave a lot of freedom for constructing an approximate polytopal DR. In sections 3.2.3 and 3.2.4 we will consider DR approximations found in the literature in light of the four aforementioned types of fluxing errors. But first we will analyse how the fluxing errors relate to the boundedness of the volume fraction.

3.2.2. Boundedness of the volume fraction

The partial volume fluxes, which were defined in eq. (19), allow the interface advection equation (16) to be restated as

$$|c|(\alpha^{\pi,(n+1)} - \alpha^{\pi,(n)}) = -\delta t \sum_{f \in \mathcal{F}(c)} o_{c,f} |f| \sum_{b \in \mathcal{C}^2(f)} \bar{v}_{f,b}^{\pi,(n)} = |c|(V_c^{+,\pi} - V_c^{-,\pi}), \quad (24)$$

where the non-negative in- and outgoing volume through the boundary of the control volume c , denoted by $V_c^{+,\pi}$ and $V_c^{-,\pi}$ respectively, are defined as

$$V_c^{\pm,\pi} := \pm \frac{\delta t}{|c|} \sum_{b \in \mathcal{C}(c)} \left[- \sum_{f \in \mathcal{F}(c)} o_{c,f} |f| \bar{v}_{f,b}^{\pi,(n)} \right]^{\pm}. \quad (25)$$

Here $\mathcal{C}(c)$ are the control volumes neighbouring c that share at least one node with c (i.e. 3^d control volumes if the mesh is rectilinear), and $[x]^+, [x]^-$ denote the positive and negative part respectively of x . Note that we have swapped the order of summation in eq. (24), which implies that fluid that is merely in transit, and therefore results in two contributions of opposite sign, does not affect the in- and outgoing volumes.

The following theorem, which will also be crucial in section 4, shows that bounded outgoing flow can be guaranteed provided that the approximate DRs do not contain some of the errors that were discussed in section 3.2.1. A proof is found in Appendix B.

Theorem 1 (Bounded outflow). *The outgoing flow is bounded by the π -phase volume fraction contained in the control volume c at $t = t^{(n)}$*

$$V^{-,\pi} \leq \alpha^{\pi,(n)}, \quad (26)$$

provided that the approximate DRs do not contain any flux overlap nor transit errors.

Provided with the result of theorem 1 we can now easily show that bounded outflow, combined with an absence of flux volume errors, results in boundedness of the volume fraction.

Corollary 1 (Boundedness of the volume fraction). *Suppose that we advect the liquid phase. An absence of flux overlap and transit errors implies that the liquid volume fraction is bounded from below*

$$\alpha^{l,(n+1)} \geq V^{+,l} \geq 0. \quad (27)$$

If additionally no flux volume errors are made then the liquid volume fraction is bounded from above as well

$$\alpha^{l,(n+1)} \leq 1 - V^{+,g} \leq 1.$$

Proof. The assumption that no flux overlap nor transit errors are made allows the use of theorem 1 (with $\pi = l$), which implies that the non-negative ingoing flow is bounded by the phase volume at $t = t^{(n+1)}$

$$V^{+,l} \stackrel{(24)}{=} \alpha^{l,(n+1)} - (\alpha^{l,(n)} - V^{-,l}) \stackrel{(26)}{\leq} \alpha^{l,(n+1)}, \quad (28)$$

and thus shows that eq. (27) holds.

Satisfying eq. (23) exactly, and thereby preventing flux volume errors to be made, ensures that implementing eq. (16) for the liquid phase yields the same interface evolution as one would obtain for the gas phase, since

$$\begin{aligned} \alpha^{g,(n+1)} - \alpha^{g,(n)} + \delta t \mathfrak{D} \bar{v}^{g,(n)} &= (1 - \alpha^{l,(n+1)}) - (1 - \alpha^{l,(n)}) + \delta t (\mathfrak{D} \{\bar{v}\}^{(n)} - \mathfrak{D} \bar{v}^{l,(n)}) \\ &\stackrel{(22)}{=} - \left[\alpha^{l,(n+1)} - \alpha^{l,(n)} + \delta t \mathfrak{D} \bar{v}^{l,(n)} \right] \\ &\stackrel{(16)}{=} 0. \end{aligned}$$

Hence we can again make use of theorem 1, but now with $\pi = g$, to find that the gas volume fraction is bounded from below as well

$$\alpha^{g,(n+1)} \geq V^{+,g},$$

where we have used the same argument as we did in eq. (28). We then use that the volume fractions add up to one, $\{\alpha^{(n+1)}\} = 1$, to find that the liquid volume fraction is indeed bounded from above

$$\alpha^{l,(n+1)} = 1 - \alpha^{g,(n+1)} \leq 1 - V^{+,g}.$$

□

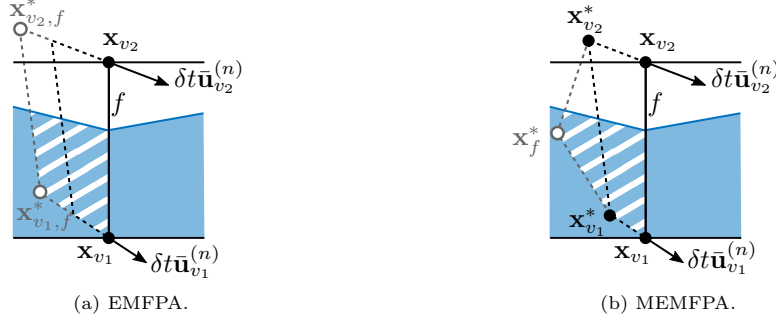


Figure 9: Example two-dimensional DRs with an exaggerated correction. The black dashed polygon corresponds to the DR without enforcing eq. (23) (i.e. $\delta t^* = 0$ in eq. (29)), whereas the gray polygon corresponds to the correction.

We will now consider a few DR approximation methods from the literature, and discuss their properties regarding the different types of fluxing errors. This then allows us, by making use of corollary 1, to guarantee boundedness of the volume fraction for some of these methods.

3.2.3. Two-dimensional approximate donating regions

Let's first consider the naive construction of a two-dimensional donating region. A face f is defined by its two vertices $\mathbf{x}_{v_1}, \mathbf{x}_{v_2}$, for $v_1, v_2 \in \mathcal{V}(f)$, where $\mathcal{V}(f)$ are the nodes of f . Using bilinear interpolation we approximate the velocity at each of the vertices, resulting in $\bar{\mathbf{u}}^{(n)} \in [\mathcal{V}^h]^d$. Simply using $\mathbf{x}_v^* = \mathbf{x}_v - \delta t \bar{\mathbf{u}}_v^{(n)}$ as the remapped (i.e. integrated backwards in time) vertices to complete the definition of the DR (see the black dashed polygon in fig. 9a) would result in a DR which avoids the flux overlap, gap and transit errors (assuming a simple CFL condition is satisfied). However a flux volume error is still made, and therefore the result of corollary 1 does not guarantee that the resulting volume fraction is bounded from above.

The edge-matched flux polygon advection (EMFPA) [22] method proposes to fix the aforementioned flux volume error by a novel modification of the DR. They propose to shift the remapped face, i.e. the face of the DR which is defined by $\mathbf{x}_{v_1}^*, \mathbf{x}_{v_2}^*$, in such a way that the volume of the resulting DR matches the total volume flux, as stated in eq. (23). The proposed modification yields the following definition of the remapped vertices

$$\mathbf{x}_{v,f}^* = \mathbf{x}_v - (\delta t + \delta t_{v,f}^*) \bar{\mathbf{u}}_v^{(n)}, \quad (29)$$

where $\delta t_{v,f}^*$ is a correction which is defined such that the remapped face tangent is invariant under this correction

$$\mathbf{x}_{v_2,f}^* - \mathbf{x}_{v_1,f}^* \parallel \mathbf{x}_{v_2}^* - \mathbf{x}_{v_1}^*, \quad (30)$$

and such that eq. (23) holds, see also fig. 9a. Hence per face f we find two equations (given by eqs. (23) and (30)) for the two unknown values of $\delta t_{v,f}^*$. This results in a scalar quadratic polynomial which has real roots except in some degenerate cases.

The EMFPA method can however commit a flux transit error because \mathbf{x}_v^* is not uniquely defined: the position of the corner of the DR depends on which face f is being considered. It follows that the EMFPA method does not necessarily lead to bounded volume fractions (neither from below nor from above) since the assumptions of corollary 1 do not hold.

In Owkes and Desjardins [24] a modification to the EMFPA method is proposed. Rather than imposing eq. (23) by making use of eq. (29), a fifth vertex is added at the centroid of the

remapped face

$$\mathbf{x}_f^* = \frac{1}{|\mathcal{V}(f)|} \sum_{v \in \mathcal{V}(f)} \mathbf{x}_v^* + \delta t_f^* \mathbf{n}_f^*,$$

where \mathbf{n}_f^* is the vector normal to $\mathbf{x}_{v_2}^* - \mathbf{x}_{v_1}^*$. The signed area of the resulting polygon, consisting of five vertices, is then, up to a constant, a linear function of δt_f^* and therefore we can easily find a δt_f^* for which eq. (23) holds. A suitable δt_f^* exists if and only if $\mathbf{x}_{v_1}^* \neq \mathbf{x}_{v_2}^*$. An example is shown in fig. 9b.

This approach alleviates any flux transit errors because the remapped vertex is now uniquely defined (contrary to the remapped vertex, given by eq. (29), which was used in the EMFPA method). Moreover it is still ensured that no flux volume errors are made by ensuring that eq. (23) holds. Hence none of the discussed fluxing errors are made and therefore corollary 1 ensures boundedness of the volume fraction. There was no name provided to the methods proposed in [24], and therefore we will refer to both the 2D and 3D method as the modified EMFPA (MEMFPA) method.

3.2.4. Three-dimensional approximate donating regions

The face matched flux polyhedron advection (FMFPA) method [14] is a 3D generalisation of the EMFPA method. The additional challenge in 3D is to ensure that the faces of the approximate DR remain planar. The FMFPA method succeeds in doing so, however this is at the cost of making flux overlap, gap as well as transit errors. For this reason we use the 3D equivalent of the MEMFPA method instead, as proposed by Owkes and Desjardins [24].

In 3D, the resulting DR is in general no longer convex, and therefore the authors of [24] propose a tetrahedralisation of the non-convex polyhedron such that routines suitable only for convex polyhedra can be used to compute the intersection volume eq. (17). We instead use the VOFTools 5 toolbox [23], which was kindly provided to us by its authors. This toolbox is able to perform intersections of non-convex polyhedra and therefore we do not need to tetrahedralise our polyhedron prior to intersection.

3.2.5. The CFL constraint

We will use the following CFL condition

$$\max_{c \in \mathcal{C}} \nu_c < \nu^\dagger, \quad (31)$$

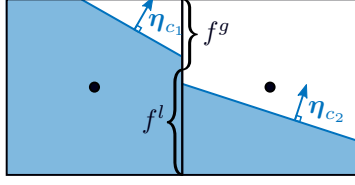
where the CFL limit is usually set to $\nu^\dagger = \frac{3}{4}$ and ν_c denotes the local control volume CFL number, which is defined as

$$\nu_c := \frac{\delta t}{|c|} \sum_{f \in \mathcal{F}(c)} \left[-o_{c,f} |f| \bar{u}_f^{(n)} \right]^+. \quad (32)$$

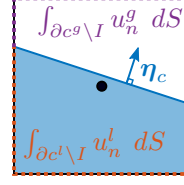
If a DR does not self-intersect, and hence has only one part of a single orientation, then the volume flux is bounded by the velocity $|\bar{v}^\pi| \leq |\bar{u}|$. The CFL condition eq. (31) then ensures that the change in volume fraction does not exceed ν_c

$$\pm (\alpha_c^{\pi, (n+1)} - \alpha_c^{\pi, (n)}) = \frac{\delta t}{|c|} \sum_{f \in \mathcal{F}(c)} \mp o_{c,f} |f| \bar{v}_f^{\pi, (n)} \leq \pm \frac{\delta t}{|c|} \sum_{f \in \mathcal{F}(c)} \left[-o_{c,f} |f| \bar{v}_f^{\pi, (n)} \right]^\pm \leq \nu_c, \quad (33)$$

which follows from eq. (16). These bounds do not always hold (a DR is permitted to self-intersect), but it illustrates the usefulness of the CFL condition (31). We find that in practise the bound eq. (33) holds almost always, and always holds when replacing ν_c by ν^\dagger .



(a) Definition of the face aperture.



(b) Boundary integral split into two parts.

Figure 10: Illustration of the cut-cell method applied to the approximation of the divergence constraint given by eq. (38).

3.3. Application to mass transport (one-velocity model)

Provided with a discretisation of eq. (11) we can now formulate the resulting equation which governs mass transport. We define the mass flux $\bar{m}^\pi \in \mathcal{F}^h$ as follows

$$\bar{m}^\pi := \rho^\pi \bar{v}^\pi. \quad (34)$$

We find that conservation of the centred mass is given by

$$\frac{(\alpha\rho)^{\pi,(n+1)} - (\alpha\rho)^{\pi,(n)}}{\delta t} + \mathfrak{A}[\bar{m}^\pi]1 = 0, \quad (35)$$

which follows from multiplying eq. (16) by the constant ρ^π . Here we have defined the advection operator $\mathfrak{A}[m] : \mathcal{C}^h \rightarrow \mathcal{C}^h$ as

$$\mathfrak{A}[m]\varphi := \mathfrak{D}(m\mathfrak{F}\varphi), \quad (36)$$

where $\mathfrak{F} : \mathcal{C}^h \rightarrow \mathcal{F}^h$ denotes the flux interpolant for which the staggered equivalent will be defined in section 4. For now it is sufficient to know that this flux interpolant will interpolate a constant field exactly: $\mathfrak{F}1 = 1$.

3.4. Geometric VOF for the two-velocity model

We will now consider the advection of the interface in the presence of a velocity discontinuity. That is, we have two staggered velocity fields $u^l, u^g \in \mathcal{F}^h$ where a value u_f^π exists if and only if the corresponding staggered volume fraction $\tilde{\alpha}_f^\pi \in \mathcal{F}^h$ is non-zero. The staggered volume fraction $\tilde{\alpha}^\pi \in \mathcal{F}^h$ is defined as the volume weighted average of the centred volume fraction

$$\tilde{\alpha}^\pi := \mathfrak{I}\alpha^\pi. \quad (37)$$

The two velocity fields are continuous in the interface normal direction (see eq. (2)), and the movement of the interface depends only on this interface normal component. Therefore we are free to use either the liquid velocity, gas velocity, or a linear combination thereof for the advection of the interface. We choose to advect the interface using the liquid velocity field, corresponding to the heaviest of the two phases, and track the liquid volume fraction field.

The velocities u^l, u^g are divergence free in the sense of eq. (12). The divergence constraint eq. (12) can be written as a sum of two boundary integrals, where we sharply distinguish the integration over the liquid and gaseous parts of the boundary

$$\int_{\partial c} u_n dS = \int_{\partial c^l \setminus I} u_n^l dS + \int_{\partial c^g \setminus I} u_n^g dS.$$

Hence for the sharp discretisation of the boundary integral we need to sharply identify which part of a face $f \subset \partial c$ is inside the liquid, and which part is in the gas phase. To this end we

introduce the face aperture $a^\pi \in \mathcal{F}^h$ which equals the fraction of the face that is occupied by the π -phase

$$a_f^{\pi,(n)} := \frac{|f \cap \Omega^{\pi,(n)}|}{|f|},$$

with¹ $\{\!\{a^{(n)}\}\!\} = 1$. Note that since a piecewise reconstruction of the interface is used, the face aperture is averaged from the two approximations from each side of the face, see also fig. 10a.

The face apertures allow for the following cut-cell [5] approximation of eq. (12)

$$|c|\mathfrak{D}(\{\!\{au\}\!\})_c = 0, \quad (38)$$

which will be used in a future paper to impose the divergence constraint on the velocity field. The cut-cell divergence operator is illustrated in fig. 10b. Using this divergence constraint implies that the divergence per phase does not vanish at the interface: $\mathfrak{D}u^\pi \neq 0$, and we can therefore not directly re-use the previously discussed interface advection method, because an absence of flux volume errors cannot be guaranteed, resulting in a loss of boundedness according to corollary 1.

Instead, we propose to solve the following additional Poisson problem, which projects the liquid velocity field u^l into the space of divergence free velocity fields

$$\begin{cases} \hat{u}_f^{l,(n)} = u_f^{l,(n)} - (\mathfrak{S}\hat{p})_f & \forall f \in \mathcal{F} \quad \text{for which } \tilde{\alpha}_f^{l,(n)} > 0 \\ (\mathfrak{D}\hat{u}^{l,(n)})_c = 0 & \forall c \in \mathcal{C} \quad \text{for which } \alpha_c^{l,(n)} > 0 \\ \hat{p}_c = 0 & \forall c \in \mathcal{C} \quad \text{for which } \alpha_c^{l,(n)} = 0 \end{cases},$$

resulting in the ‘extrapolated’ velocity field $\hat{u}^{l,(n)}$. Recall that the gradient operator \mathfrak{S} was defined in eq. (5). We will now show that the use of this Poisson problem is sufficient for guaranteeing boundedness of the volume fraction. If the centred volume fraction is non-zero $\alpha_c^{l,(n)} > 0$ then $(\mathfrak{D}\hat{u})_c^{l,(n)} = 0$ and therefore no flux volume errors are made, resulting in boundedness of the volume fraction according to corollary 1. On the other hand, if the centred volume fraction is initially zero $\alpha_c^{l,(n)} = 0$, then flux volume errors are made because the velocity field is not divergence free (note that missing velocities whose staggered volume fraction is zero are computed using constant extrapolation), but theorem 1 still guarantees that the volume fraction will be bounded from below. Moreover, by the CFL constraint eqs. (31) and (32) as well as eq. (33) we find that $\alpha_c^{\pi,(n+1)} \leq \nu^\dagger \leq 1$.

We can therefore apply the dimensionally unsplit interface advection method, as discussed in section 3.2, where we use the extrapolated velocity field $\hat{u}^{l,(n)}$. The resulting DRs are denoted as $\hat{\Delta}_f^{l,(n)}$. From these DRs we define the following liquid volume flux (cf. eq. (17))

$$\delta t |f| \hat{v}_f^{l,(n)} := M_0(\hat{\Delta}_f^{l,(n)} \cap \Omega^{l,(n)}),$$

resulting in the following interface advection equation (cf. eq. (16))

$$\frac{\alpha^{l,(n+1)} - \alpha^{l,(n)}}{\delta t} + \mathfrak{D}\hat{v}^{l,(n)} = 0. \quad (39)$$

¹Our proposed methods allow for the presence of arbitrary geometry, which is modelled implicitly using the cut-cell method [17, 8, 5]. This means that in such cut-cells we find $\{\!\{a^{(n)}\}\!\} < 1$, as the remainder of the face is filled by the geometry. Throughout this paper it will however be assumed that each control volume consists entirely of liquid and/or gas for ease of discussion.

3.5. Application to mass transport (two-velocity model)

For the two-velocity formulation we find that the transport of the centred liquid mass is given by

$$\frac{(\alpha\rho)^{l,(n+1)} - (\alpha\rho)^{l,(n)}}{\delta t} + \mathfrak{A}[\widehat{m}^l]1 = 0, \quad (40)$$

which follows from multiplying eq. (39) by ρ^l . Here the liquid mass flux is defined as

$$\widehat{m}^l := \rho^l \widehat{v}^l.$$

Note that the divergence free liquid velocity $\widehat{u}^{l,(n)}$ is available only inside the liquid phase (only on those faces f for which $\widetilde{\alpha}_f^{l,(n)} > 0$), and therefore the gas mass fluxes inside the gas phase cannot be obtained using $\widehat{u}^{l,(n)}$. On the other hand we do know the gas mass inside the gas phase

$$(\alpha\rho)^{g,(n+1)} = (1 - \alpha^{l,(n+1)})\rho^g, \quad (41)$$

which is conserved as a consequence of $\alpha^{l,(n+1)}$ being conserved.

For the transport of momentum, which will be discussed in section 4, we will need to know not only the gas mass, but also the gas mass fluxes inside the gas phase, and to this end we define the gas mass flux as

$$m^g := \rho^g v^g,$$

where the volume fluxes v^g follow from using the DR method inside the gas phase with the gas velocity field u^g . Hence on faces at the interface we compute two DRs: one DR is constructed using the divergence free liquid velocity \widehat{u}^l , resulting in the liquid mass fluxes \widehat{m}^l , and another DR is constructed using the gas velocity u^g , resulting in the gas mass fluxes m^g . The resulting centred mass, according to the gas mass fluxes, is denoted by $(\alpha\rho)^{*,\pi}$, for which

$$\frac{(\alpha\rho)^{g,*} - (\alpha\rho)^{g,(n)}}{\delta t} + \mathfrak{A}[m^g]1 = 0. \quad (42)$$

The gas velocity field is not divergence free (contrary to \widehat{u}^l), but if we do not enforce the volume of the resulting DRs, and thereby permit flux volume errors, then this is not a problem: the presence of flux volume errors means that the volume fraction may exceed one, but it is still ensured to be bounded from below by zero according to corollary 1. Note that $\alpha^{g,*}$ as well as $1 - \alpha^{l,(n+1)}$ are consistent estimates of the gas volume fraction at $t = t^{(n+1)}$. However only the latter, by which the interface is defined, is bounded from above as well as below.

4. Transport of momentum

We will now focus our attention on the conservative advection of some (possibly discontinuous) staggered (i.e. defined at the faces of the control volume) scalar φ , which is modelled by eq. (3). The control volume now coincides with the staggered control volume $\omega = \omega_f$, resulting in

$$\int_{\omega_f^{\pi,(n+1)}} \rho^\pi \varphi^\pi dV - \int_{\omega_f^{\pi,(n)}} \rho^\pi \varphi^\pi dV + \sum_{g \in \mathcal{G}(\omega_f)} \int_{t^{(n)}}^{t^{(n+1)}} \int_{g^\pi(t)} \rho^\pi u_n^\pi \varphi^\pi dS dt = 0. \quad (43)$$

We denote the staggered *advected* quantity by $\widetilde{\varphi}^\pi \in \mathcal{F}^h$ to emphasise the distinction with the *advecting* velocity field u^π . For momentum transport in the one-velocity formulation we let $\widetilde{\varphi}^\pi = \bar{u}$, and in the two-velocity formulation we use $\widetilde{\varphi}^\pi = u^\pi$. We will first consider the one-velocity formulation.

An approximation of eq. (43) consists of the approximation of both the volume integral of $(\rho\varphi)^\pi$ as well as the space-time integral of $\rho^\pi \bar{u}_n \varphi^\pi$. We choose to approximate the former by the product of the integration volume (given by $|\omega_f| \tilde{\alpha}_f^{\pi,(n)}$) with the value of $(\rho\tilde{\varphi})^\pi$ in the control volume centroid

$$|\omega_f|(\tilde{\alpha}\rho\tilde{\varphi})_f^{\pi,(n)} \approx \int_{\omega_f^{\pi,(n)}} (\rho\varphi)^{\pi,(n)} dV,$$

where $\tilde{\varphi}^\pi \in \mathcal{F}^h$ is such that

$$\tilde{\varphi}_f^{\pi,(n)} \approx \varphi^\pi(t^{(n)}, \mathbf{x}_f),$$

and $\tilde{\alpha}$ denotes the staggered volume fraction function as defined in eq. (37). The space-time integral is similarly approximated as the product of the mass flux $\tilde{m}^{\pi,(n)} \in \mathcal{G}^h$ (recall that \mathcal{G} is the set of faces of the staggered control volumes) with the value of φ^π at the centroid of the DR (cf. eq. (13))

$$\delta t |f| \tilde{m}_g^{\pi,(n)} (\tilde{\mathfrak{F}} \tilde{\varphi}^{\pi,(n)})_g \approx \int_{t^{(n)}}^{t^{(n+1)}} \int_{g^\pi(t)} \rho^\pi \bar{u}_n \varphi^\pi dS dt, \quad (44)$$

where $\tilde{\mathfrak{F}} : \mathcal{F}^h \rightarrow \mathcal{G}^h$ is the flux interpolant which interpolates to the centroid of the DR (see fig. 11)

$$(\tilde{\mathfrak{F}} \tilde{\varphi}^{\pi,(n)})_g \approx \varphi^\pi(t^{(n)}, \mathbf{C}_g^{(n)}).$$

The DR, which will be denoted by $\tilde{\Delta}_g^{(n)}$, is now based on the face g of a staggered control volume ω_f , and is formally defined such that (cf. eq. (13))

$$M_0(\tilde{\Delta}_g^{(n)} \cap \Omega^{\pi,(n)}) = \int_{t^{(n)}}^{t^{(n+1)}} \int_{g^\pi(t)} \bar{u}_n dS dt,$$

holds. The centroid of the DR $\tilde{\Delta}_g^{(n)}$ is denoted by $\mathbf{C}_g^{(n)}$.

In what follows we discuss the approximation of the newly introduced terms in eq. (44): the mass flux \tilde{m} as well as the flux interpolant $\tilde{\mathfrak{F}}$. We will then first apply this to the one-velocity formulation, and subsequently generalise the proposed method to the two-velocity formulation.

4.1. Mass flux computation

There are several approaches to compute the staggered mass flux, or equivalently, the staggered volume flux. Originally, Rudman [30] proposed a dimensionally split advection method wherein the volume fraction field was defined on a refined grid: every control volume was split into 2^d control volumes. Subsequently the mass fluxes were geometrically computed on the faces of each of the refined control volumes. Provided with the mass fluxes on a refined grid, one can compute the mass fluxes on the original grid by simply adding the corresponding refined mass fluxes. In this way the mass fluxes of the centred as well as staggered control volumes can all be computed directly from the refined mass fluxes. A similar approach was followed by Zuzio et al. [43] for a dimensionally split advection method, and by Owkes and Desjardins [25] for a dimensionally unsplit advection method.

Alternatively one can construct DRs directly on the faces of the staggered control volume ω_f , and define the mass fluxes for the staggered control volume in this way, resulting in

$$\delta t |g| \tilde{m}_g^\pi = \rho^\pi M_0(\tilde{\Delta}_g^{(n)} \cap \Omega^{\pi,(n)}).$$

This would result in the following staggered advection of $\tilde{\varphi}^\pi$

$$\frac{(\tilde{\alpha}\rho)^{\pi,*}\tilde{\varphi}^{\pi,(n+1)} - (\tilde{\alpha}\rho\tilde{\varphi})^{\pi,(n)}}{\delta t} + \tilde{\mathfrak{D}}\left(\tilde{m}^{\pi,(n)}\tilde{\mathfrak{F}}\tilde{\varphi}^{\pi,(n)}\right) = 0, \quad (45)$$

where the staggered divergence operator $\tilde{\mathfrak{D}}$ is as defined in eq. (7). This approach is followed by Arrufat et al. [1] where it is applied to a dimensionally split advection method. Note that in following this approach, the staggered volume fraction must be defined geometrically from the intersection of the staggered control volume with the phase domain. The downside of this approach is that the staggered mass, which follows from letting $\tilde{\varphi} = 1$ in eq. (45), will become out of sync with the centred mass which itself evolves according to eq. (35). This means that the staggered mass must be reset after every time step, resulting in a loss of momentum conservation.

We instead propose a third alternative which is based on simply averaging the mass fluxes (recall that the interpolant $\tilde{\mathfrak{I}}$ is as defined in eq. (8))

$$\tilde{m}^\pi := \tilde{\mathfrak{I}}\bar{m}^\pi, \quad (46)$$

for which the staggered advection equation is given by

$$\frac{(\tilde{\alpha}\rho\tilde{\varphi})^{\pi,(n+1)} - (\tilde{\alpha}\rho\tilde{\varphi})^{\pi,(n)}}{\delta t} + \tilde{\mathfrak{A}}[\tilde{m}^{\pi,(n)}]\tilde{\varphi}^{\pi,(n)} = 0, \quad (47)$$

where we define the staggered advection operator $\tilde{\mathfrak{A}}[m] : \mathcal{F}^h \rightarrow \mathcal{F}^h$ as

$$\tilde{\mathfrak{A}}[m]\tilde{\varphi} := \tilde{\mathfrak{D}}\left((\tilde{\mathfrak{I}}m)(\tilde{\mathfrak{F}}\tilde{\varphi})\right). \quad (48)$$

In Appendix C we show that for this advection operator the corresponding semi-discrete formulation preserves quadratic invariants, such as kinetic energy, provided that the LW flux interpolant (which will be introduced next) is used.

This approach is reminiscent of the flux interpolation used in the cut-cell method from Dröge and Versteppen [9]. Therein a symmetry preserving convection operator near a solid boundary (rather than a moving phase interface) is proposed where the volume fluxes used in the convection operator are simply averaged from the volume fluxes that are defined on the faces of the centred control volumes. The advantage of doing so, is that the divergence operator, which is based on the volume fluxes of the centred control volumes, shows up in the convection operator, resulting in a skew-symmetric operator if the volume fluxes are divergence free. Simply averaging the volume fluxes may seem inconsistent at first, but a geometric interpretation is provided in [9, 4].

Recall from eq. (9) that the centred and staggered divergence operators are related, and therefore (moreover using eqs. (36) and (48))

$$\tilde{\mathfrak{A}}[m]1 = \mathfrak{I}(\mathfrak{A}[m]1), \quad \forall m \in \mathcal{F}^h. \quad (49)$$

This implies that the staggered mass transport equation (which follows from substituting $\tilde{\varphi} = 1$ in eq. (47)) can also be written as

$$\frac{(\tilde{\alpha}\rho)^{\pi,(n+1)} - (\tilde{\alpha}\rho)^{\pi,(n)}}{\delta t} + \mathfrak{I}(\mathfrak{A}[\tilde{m}^{\pi,(n)}]1) = 0,$$

and therefore the evolution equation for the staggered mass can equivalently be obtained from application of the interpolation operator \mathfrak{I} to eq. (35). This means that, unlike the method proposed in Arrufat et al. [1], we need not reset the staggered mass after every time step to ensure that it remains in sync with the centred mass, thereby obtaining exact conservation of linear momentum, without the need for subgrid mass fluxes as was used by e.g. Rudman [30].

4.2. Flux interpolation

All that remains for the discretisation of eq. (43) is to define the flux interpolant, which interpolates the value of $\tilde{\varphi}^\pi$ to the centroid of the DR for each of the faces of a control volume. We let the centroid of the DR be approximated by

$$\mathbf{C}_g^{(n)} := \mathbf{x}_g - \frac{\delta t}{2} \tilde{\mathbf{u}}_g^{(n)},$$

where $\tilde{\mathbf{u}}^{(n)} \in [\mathcal{G}^h]^d$ denotes an interpolated vector-valued velocity.

From eq. (47) it follows that the value of $\tilde{\varphi}^{\pi, (n+1)}$ can be computed as follows

$$\tilde{\varphi}^{\pi, (n+1)} = \frac{(\tilde{\alpha}\rho\tilde{\varphi})^{\pi, (n)} - \delta t \tilde{\mathfrak{A}}[\tilde{m}^{\pi, (n)}] \tilde{\varphi}^{\pi, (n)}}{(\tilde{\alpha}\rho)^{\pi, (n+1)}}. \quad (50)$$

Hence if a staggered control volume is drained of the π -phase during a single time step, i.e. $\tilde{\alpha}_f^{\pi, (n+1)} \rightarrow 0$, we must somehow guarantee that the numerator in the right-hand side of eq. (50) tends to zero as well to make sure that $\tilde{\varphi}_f^{\pi, (n+1)}$ is well-defined. In terms of the transport of momentum this relates to ensuring that the velocity can be obtained from the momentum and mass without any problems. We will refer to this as the ‘boundedness property’ of the flux interpolant

We will first discuss the construction of the flux interpolant away from the interface, that is, where we can guarantee that $\tilde{\alpha}_f^{\pi, (n+1)}$ does not vanish. Then we will consider a different (more dissipative) flux interpolant which is to be used at the interface, and is guaranteed to be bounded. Finally we will switch between both flux interpolants in such a way that we only use the more dissipative flux interpolant when necessary, while still guaranteeing boundedness.

4.2.1. Flux interpolant away from the interface

Away from the interface we need not worry about boundedness, and therefore the construction of the flux interpolant is focused on obtaining a second-order accurate approximation of φ^π at the centroid of the DR. The flux interpolant that we propose is constructed in two steps: first we compute one downwind and two upwind approximations of φ^π that all lie on a single line containing the centroid of the DR, then we interpolate along this line to obtain a second-order approximation of φ^π at the centroid of the DR.

We let the downwind approximation, which we denote by $(\tilde{\mathfrak{U}}_0 \tilde{\varphi}^\pi)_g$, coincide with the value $\tilde{\varphi}_f^\pi$, where $f \in \mathcal{F}^\omega(g)$ (the set $\mathcal{F}^\omega(g)$ is illustrated in fig. 5b) corresponds to the staggered control volume ω_f which is downwind from g , as illustrated in fig. 11. Since the centroid of the DR is assumed to lie on the interpolation line, it follows that $(\tilde{\mathfrak{U}}_0 \mathbf{x})_g$ and $\mathbf{C}_g^{(n)}$ entirely define the interpolation line as indicated by the dashed line in fig. 11. The first upwind value $(\tilde{\mathfrak{U}}_1 \tilde{\varphi}^\pi)_g$ is obtained via (bi)linear interpolation using the two (four in 3D) neighbouring values of $\tilde{\varphi}^\pi$ that lie in the plane with normal \mathbf{n}_g and passes through the centroid of the upwind control volume. The linear interpolation is indicated by the dotted vertical lines in fig. 11. The second upwind value $(\tilde{\mathfrak{U}}_2 \tilde{\varphi}^\pi)_g$ is computed similarly (when needed). Note that it may happen that the upwind value $(\tilde{\mathfrak{U}}_2 \tilde{\varphi}^\pi)_g$ is missing because the corresponding staggered control volumes do not contain the π -phase, in this case we resort to using only $(\tilde{\mathfrak{U}}_1 \tilde{\varphi}^\pi)_g$.

We are now ready to perform the second interpolation step. The simplest second-order accurate approximation to the value of $\tilde{\varphi}^\pi$ at the centroid of the DR is given by (assuming a uniform mesh)

$$\tilde{\mathfrak{F}}^{\text{LW}} \tilde{\varphi} := \frac{1}{2} (1 - \nu) \tilde{\mathfrak{U}}_0 \tilde{\varphi} + \frac{1}{2} (1 + \nu) \tilde{\mathfrak{U}}_1 \tilde{\varphi}, \quad (51)$$

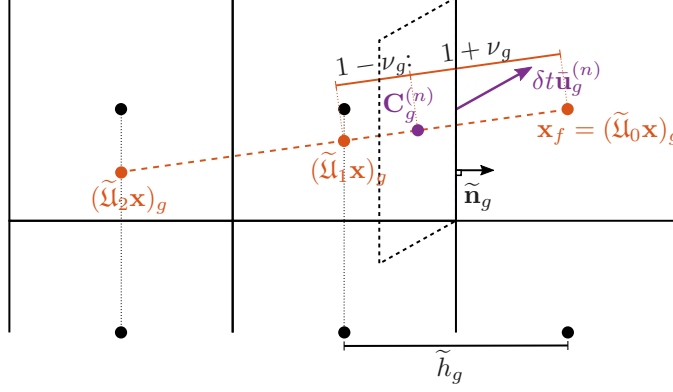


Figure 11: Example of a DR (black dashed lines) defined on some face $g \in \mathcal{G}(\omega_f)$. The downwind interpolant $\tilde{\mathcal{U}}_0$ simply yields the value downwind of the face g , whereas the i -th upwind interpolant $\tilde{\mathcal{U}}_i$ is defined as the interpolant that linearly interpolates along the i -th black dotted line to the point of intersection with the red dashed line, for $i = 1, 2$. The red dashed interpolation line is defined by the downwind node \mathbf{x}_f as well as the centroid $\mathbf{C}_g^{(n)}$ of the DR.

where $\nu^{(n)} \in \mathcal{G}^h$ denotes the CFL number per face and is given by

$$\nu^{(n)} := \frac{\delta t \tilde{\mathcal{J}} \bar{u}^{(n)}}{\tilde{h}}.$$

Equation (51) can be seen as a multidimensional generalisation of the Lax–Wendroff (LW) flux interpolant (see e.g. Leveque [19]). The second upwind value can be included in the approximation in the following way

$$\tilde{\mathfrak{F}}^{\text{Method}} \tilde{\varphi} := \tilde{\mathcal{U}}_1 \tilde{\varphi} + \frac{1}{2} (1 - \nu) \Psi^{\text{Method}}(\iota) (\tilde{\mathcal{U}}_0 \tilde{\varphi} - \tilde{\mathcal{U}}_1 \tilde{\varphi}), \quad (52)$$

where $\Psi^{\text{Method}}(\iota)$ denotes the flux limiter function which is a function of the ratio of the slopes

$$\iota = \frac{\tilde{\mathcal{U}}_1 \tilde{\varphi} - \tilde{\mathcal{U}}_2 \tilde{\varphi}}{\tilde{\mathcal{U}}_0 \tilde{\varphi} - \tilde{\mathcal{U}}_1 \tilde{\varphi}} \frac{|\tilde{\mathcal{U}}_0 \mathbf{x} - \tilde{\mathcal{U}}_1 \mathbf{x}|_2}{|\tilde{\mathcal{U}}_1 \mathbf{x} - \tilde{\mathcal{U}}_2 \mathbf{x}|_2}.$$

The following flux limiter functions [19] are considered

$$\begin{aligned} \Psi^{\text{LW}}(\iota) &:= 1 \\ \Psi^{\text{Fromm}}(\iota) &:= \frac{1 + \iota}{2} \\ \Psi^{\text{MC}}(\iota) &:= \max(0, \min(\Psi^{\text{Fromm}}(\iota), 2, 2\iota)) \\ \Psi^{\text{Upwind}}(\iota) &:= 0, \end{aligned}$$

where the LW flux simply interpolates between $\tilde{\mathcal{U}}_0 \tilde{\varphi}$ and $\tilde{\mathcal{U}}_1 \tilde{\varphi}$ and coincides with eq. (51), the Fromm flux uses the average of the central and upwind gradient, the monotonised central (MC) flux limits the Fromm flux to the TVD region of the Sweby diagram [33] (or normalised variable diagram) and the upwind flux simply uses the upwind value $\tilde{\mathcal{U}}_1 \tilde{\varphi}$. Note that only the upwind and MC fluxes are really limited.

4.2.2. Flux interpolant at the interface

Using the previously introduced flux interpolant eq. (52) near the interface may easily result in an unbounded value of $\tilde{\varphi}^\pi$ when the control volume is drained of the π -phase, even if the upwind interpolant is used.

One of the culprits of such unboundedness is the fact that fluid that is merely in transit still affects the final value of $\tilde{\varphi}^\pi$. This could be prevented by explicitly computing the volume of the fluid that is in transit and introducing a diagonal flux which bypasses the control volume c altogether. However this requires intersection of neighbouring DRs, which would be cumbersome and expensive.

To this end we now introduce the corner transport upwind (CTU) flux interpolant, for which the resulting advection method is reminiscent of the CTU method [18]. The CTU flux interpolant is defined as follows

$$(\tilde{\mathfrak{F}}^{\text{CTU}} \tilde{\varphi}^{\pi,(n)})_g := \frac{\sum_{k \in \mathcal{F}^2(g)} \tilde{v}_{g,k}^{\pi,(n)} \tilde{\varphi}_k^{\pi,(n)}}{\tilde{v}_g^{\pi,(n)}}, \quad (53)$$

where the volume fluxes $\tilde{v}^{\pi,(n)} \in \mathcal{G}^h$ are interpolated as (cf. eq. (46))

$$\tilde{v}^{\pi,(n)} := \tilde{\mathcal{J}} \bar{v}^{\pi,(n)}, \quad (54)$$

and $\mathcal{F}^2(g) \subset \mathcal{F}$ denotes the set of faces whose corresponding staggered control volumes share at least one vertex with the face $g \in \mathcal{G}$ (hence resulting in $2 \times 3^{d-1}$ faces on a rectilinear mesh). The partial volume fluxes (from eq. (19)) are interpolated in a similar fashion. This results in a $\tilde{\varphi}^\pi$ -flux which is simply the sum over all the signed areas multiplied by their respective $\tilde{\varphi}^\pi$ -values. In particular this means that if neighbouring DRs overlap with opposite relative orientation, then their combined contribution does not contain any contribution from this overlapping region.

The following lemma shows that the CTU flux interpolant always results in boundedness, under the assumption that the DRs do not contain any flux overlap nor transit errors. Here the set $\mathcal{F}(f)$ denotes those faces whose corresponding staggered control volume shares at least one vertex with ω_f (hence resulting in 3^d neighbouring faces on a rectilinear mesh).

Lemma 2 (Boundedness of the CTU flux interpolant). *The CTU flux interpolant eq. (53) results in boundedness of $\tilde{\varphi}^{\pi,(n+1)}$ in the following sense*

$$\left| \tilde{\varphi}_f^{\pi,(n+1)} - \tilde{\varphi}_f^{\pi,(n)} \right| \leq \max_{k \in \mathcal{F}(f)} \left| \tilde{\varphi}_k^{\pi,(n)} - \tilde{\varphi}_f^{\pi,(n)} \right|,$$

provided that the approximate DRs do not contain any flux overlap nor transit errors, and that the CFL constraint given by eq. (31) is satisfied for $\nu^\dagger \leq 1$.

A proof is found in Appendix B. Note that no such result can be shown without making use of the partial volume fluxes, since for the usual volume fluxes $\bar{v}_f^{\pi,(n)}$ no equivalent of theorem 1 can be shown due to the presence of fluid which is merely in transit. It is exactly this fluid that is in transit that cancels out due to swapping the order of summation in eq. (24), and this cancellation allows for theorem 1, and thus lemma 2, to be proven.

4.2.3. The modified flux interpolant

Using the CTU flux interpolant introduced previously alleviates any issues regarding boundedness, provided that no flux overlap and transit errors are committed, but it is a rather dissipative and only first-order accurate interpolant. To this end we will now introduce the modified flux interpolant, which switches between the second-order accurate interpolant from section 4.2.1 and

the CTU flux interpolant from section 4.2.2 in a way that the latter is only used whenever it is needed to ensure boundedness. The modified flux interpolant is defined as

$$(\tilde{\mathfrak{F}}^{\text{Method}^*} \tilde{\varphi})_g^{\pi, (n)} := \begin{cases} (\tilde{\mathfrak{F}}^{\text{CTU}} \tilde{\varphi})_g^{\pi, (n)} & \text{if } \min_{f \in \mathcal{F}^\omega(g)} \tilde{\alpha}_f^{\pi, (n+1)} < \alpha^\dagger \\ (\tilde{\mathfrak{F}}^{\text{Method}} \tilde{\varphi})_g^{\pi, (n)} & \text{otherwise} \end{cases}, \quad (55)$$

for some parameter $\alpha^\dagger > 0$. If a staggered control volume ω_f results in $\tilde{\alpha}_f^{\pi, (n+1)} < \alpha^\dagger$, then each of the modified interpolant fluxes through the boundary faces $g \in \mathcal{G}(\omega_f)$ will reduce to the CTU flux, resulting in boundedness via lemma 2. And if a staggered control volumes results in $\tilde{\alpha}_f^{\pi, (n+1)} \geq \alpha^\dagger$, then the following result shows that the modified interpolant still yields some form of boundedness.

Lemma 3 (Boundedness of the modified flux interpolant). *Assuming that $\tilde{\alpha}_f^{\pi, (n+1)} \geq \alpha^\dagger$, we find that the temporal update in $\tilde{\varphi}^\pi$ is bounded in the following sense*

$$\left| \tilde{\varphi}_f^{\pi, (n+1)} - \tilde{\varphi}_f^{\pi, (n)} \right| \leq \frac{\tilde{W}_f^{+, \pi} + \tilde{W}_f^{-, \pi}}{\alpha^\dagger} \max_{g \in \mathcal{G}(\omega_f)} \left| (\tilde{\mathfrak{F}}^{\text{Method}^*} \tilde{\varphi}^{\pi, (n)})_g - \tilde{\varphi}_f^{\pi, (n)} \right|,$$

where the in- and outgoing volume, without re-ordering the summation over the partial volume fluxes, is given by

$$\tilde{W}_f^{\pm, \pi} := \pm \frac{\delta t}{|\omega_f|} \sum_{g \in \mathcal{G}(\omega_f)} \left[-\tilde{o}_{f, g} |g| \tilde{v}_g^{\pi, (n)} \right]^\pm.$$

A proof is found in Appendix B. By not using the partial volume fluxes we cannot re-order the summation over the partial volume fluxes, and therefore fluid that is merely in transit does not cancel (as was the case with the previously discussed CTU flux interpolant). This prohibits the possibility of obtaining a bound for $\tilde{W}_f^{+, \pi}$ in terms of $\tilde{\alpha}_f^{\pi, (n+1)}$, and therefore we obtain an upper bound which is inversely proportional to the assumed lower bound of $\tilde{\alpha}_f^{\pi, (n+1)}$ (denoted by α^\dagger). Moreover, if each of the DRs do not self intersect then we can directly make use of eq. (33), resulting in $\tilde{W}^{\pm, \pi} \leq \mathfrak{I}\nu$, such that the resulting bound from lemma 3 can be somewhat simplified

$$\left| \tilde{\varphi}_f^{\pi, (n+1)} - \tilde{\varphi}_f^{\pi, (n)} \right| \leq \frac{2(\mathfrak{I}\nu)_f}{\alpha^\dagger} \max_{g \in \mathcal{G}(\omega_f)} \left| (\tilde{\mathfrak{F}}^{\text{Method}^*} \tilde{\varphi}^{\pi, (n)})_g - \tilde{\varphi}_f^{\pi, (n)} \right|. \quad (56)$$

In practise this bound holds with $\mathfrak{I}\nu$ replaced by ν^\dagger , since DRs are permitted to self intersect. We will use $\alpha^\dagger = \frac{1}{2}$ (unless indicated otherwise), hence the CTU flux interpolant is used if a staggered control volume becomes less than half full.

4.3. The one-velocity formulation

When the one-velocity formulation is considered we assume continuity of the velocity field. However, the momentum transport method proposed here leads to two velocity fields to be defined at the interface after each time step (we let $\tilde{\varphi}^\pi = \bar{u}$ in eq. (47))

$$u^{\pi, (n+1)} = \frac{(\tilde{\alpha}\rho)^{\pi, (n)} \bar{u}^{(n)} - \delta t \tilde{\mathfrak{A}}[\tilde{m}^{\pi, (n)}] \bar{u}^{(n)}}{(\tilde{\alpha}\rho)^{\pi, (n+1)}},$$

which in general will not be equal $u^{l, (n+1)} \neq u^{g, (n+1)}$. Here we follow Arrufat et al. [1] and choose to define a single continuous velocity as the sum (over the phases) of the momentums divided by the sum of the masses

$$\bar{u}^{(n+1)} = \frac{\{\{\tilde{\alpha}\rho u\}\}^{(n+1)}}{\{\{\tilde{\alpha}\rho\}\}^{(n+1)}}, \quad (57)$$

which results in

$$\frac{(\{\tilde{\alpha}\rho\}\bar{u})^{(n+1)} - (\{\tilde{\alpha}\rho\}\bar{u})^{(n)}}{\delta t} + \{\{\tilde{\alpha}[\bar{m}]\bar{u}\}\}^{(n)} = 0,$$

and thus yields exact conservation of the sum (over the phases) of the total linear momentum.

4.4. The two-velocity formulation

We will use the mass fluxes \hat{m}^l, m^g , as defined in section 3.5, for the transport of mass and momentum in the two-velocity formulation, for the liquid and gas phase respectively. For the liquid phase this results in the advection method

$$\frac{(\tilde{\alpha}\rho u)^{l,(n+1)} - (\tilde{\alpha}\rho u)^{l,(n)}}{\delta t} + \mathfrak{A}[\hat{m}^{l,(n)}]u^{l,(n)} = 0. \quad (58)$$

The transport of the staggered mass follows from application of the interpolant \mathfrak{J} to the centred mass transport eq. (40), and can equivalently be obtained from eq. (58) by letting $u^l \equiv 1$ by making use of eq. (49). It follows that liquid momentum is exactly conserved as the staggered mass need not be redefined.

On the other hand, transport of gas momentum is achieved using the mass fluxes m^g , resulting in

$$\frac{\tilde{\alpha}^{g,*}(\rho u)^{g,(n+1)} - (\tilde{\alpha}\rho u)^{g,(n)}}{\delta t} + \mathfrak{A}[m^{g,(n)}]u^{g,(n)} = 0. \quad (59)$$

Contrary to the transport of liquid mass and momentum, letting $u^g \equiv 1$ in eq. (59) now does not yield the same staggered gas mass transport as one would obtain using the interpolant \mathfrak{J} applied to eq. (41). Instead, as previously discussed in section 3.5, letting $u^g \equiv 1$ in eq. (59) yields the same staggered gas mass transport as one would obtain when applying the interpolant \mathfrak{J} to eq. (42), which uses the same gas mass fluxes m^g as used in eq. (59). For obtaining a bounded value of the gas velocity we must divide the gas momentum by the gas mass which results from the same gas mass fluxes m^g , hence the one defined in eq. (42). Hence we will reset the gas mass according to eq. (41) after every time step, resulting in a loss of momentum conservation in the gas phase. We deem this to be acceptable because the gas density is much smaller than that of the liquid $\rho^g \ll \rho^l$, and therefore the loss or gain of momentum is comparatively small.

4.5. Discussion

We give an overview of momentum transport methods found in the literature, restricted to staggered formulations using a DR-based geometric VOF method, in table 1. Our proposed advection method for both the one- and two-velocity formulation has been included. All of the methods under consideration conserve the liquid as well as gas mass. Note that for the split methods often no arguments regarding boundedness were made in the respective references, which is most likely because for a dimensionally split method, a simple upwind flux corresponds to what the CTU flux would give, and therefore sufficient limiting implies boundedness. In Arrufat et al. [1] the authors mention the use of a very low CFL number (0.03) and they still report the ‘blow up’ of the solution, which is likely to be related to not taking boundedness into account.

For the dimensionally unsplit method from Owkes and Desjardins [25] we find that the CTU flux interpolant is used in a neighbourhood around the interface. This ensures boundedness, but we find that using it everywhere near the interface results in an unnecessarily dissipative flux interpolant, and we would always suggest using the modified flux interpolant as proposed in section 4.2.3 to ensure that the CTU flux interpolant is used only as much as required for ensuring boundedness.

	Unsplit?	Conservative?	# volume fluxes	# reconstructions	# velocities	Flux interpolation
Rudman [30]	N	$l + g$	$d2^{d-1}$	$d(2^d - 1)$	1	Flux limiting
Zuzio et al. [43]	N	$l + g$	$d2^{d-1}$	0	1	WENO5
Arrufat et al. [1]	N		d^2	d^2	1	QUICK/Superbee
Owkes and Desjardins [25]	Y	$l + g$	$d2^{d-1}$?	1	CTU near interface
Proposed one-velocity	Y	$l + g$	0	0	1	CTU if needed
Proposed two-velocity	Y	l	d	0	2	CTU if needed

Table 1: Overview of considered methods for the transport of a staggered momentum field, where the bold-faced methods are proposed in this paper. Conservation of ‘ $l + g$ ’ means that the sum of liquid and gas momentum is conserved, whereas ‘ l ’ means that the liquid momentum is conserved (and the gas momentum is not). We show the *additional* number of volume fluxes and interface reconstructions that are needed per centred interface control volume for the transport of momentum (excluding those needed for the advection of the interface: d for a split method and 1 for an unsplit method).

Our proposed use of interpolated mass (or equivalently, volume) fluxes results in (to the best of our knowledge) the only, dimensionally split or unsplit, staggered advection method which does not require any additional volume flux computation. Moreover the staggered advection method results in exact mass and momentum conservation (for the one-velocity formulation), sharply models the interface and ensures that quadratic invariants are preserved in the semi-discrete limit $\delta t \rightarrow 0$ if the LW flux interpolant is used (see Appendix C).

5. Validation

We will now validate the proposed staggered advection methods for both the one- and two-velocity formulation. Since we have thus far not discussed how we impose eq. (2), we will use a single and therefore continuous advecting velocity field which will be denoted by $\bar{\mathbf{u}}$. This means that for now we will use $u^g = u^l = \bar{u}$ as the advecting velocity field when the two-velocity formulation is considered. In a future paper, where the discretisation of eq. (2) will be discussed, we will consider a multitude of test cases for which $\llbracket u \rrbracket \neq 0$.

The advected field, which we will again denote by $\tilde{\varphi}^\pi \in \mathcal{F}^h$, will be discontinuous to mimic the presence of an unresolved shear layer

$$\tilde{\varphi}_x^l(t_0, \mathbf{x}) = \prod_{i=1}^d \sin(4\pi x_i), \quad \tilde{\varphi}_x^g(t_0, \mathbf{x}) = \prod_{i=1}^d \cos(2\pi x_i), \quad (60)$$

where the remaining y, z components are zero. The advection of this staggered field, for the one-velocity formulation, is performed as if it were momentum: after each time step the two fields are merged according to eq. (57), where $\rho^g/\rho^l = 10^{-3}$.

At all times we will use the modified flux interpolant as given by eq. (55).

In 2D we consider the classical vortex reverse problem [2, 29] where the interface undergoes

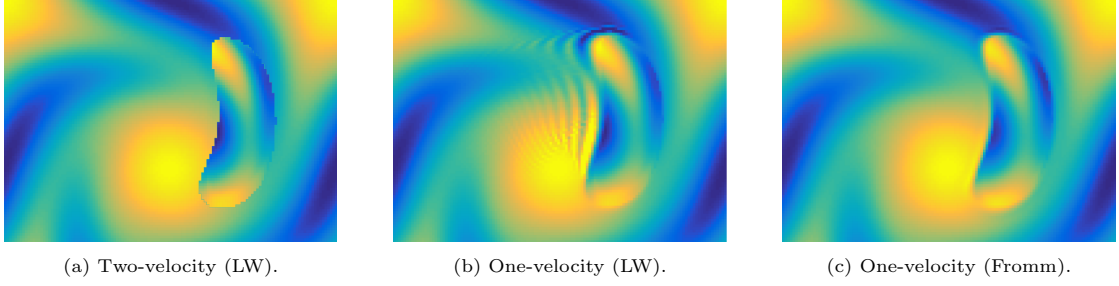


Figure 12: Example intermediate solutions to the 2D vortex reverse problem, where the field eq. (60) is passively advected along with the flow. Here $h/R \approx 1/19$.

a reversible deformation defined by the stream function

$$\bar{\psi}(t, \mathbf{x}) = \frac{\cos(\pi t/T)}{\pi} \sin(\pi x)^2 \sin(\pi y)^2.$$

The initial interface is a circle of radius $R = 0.15$ centred at $\mathbf{x}_0 = [0.5 \ 0.75]^T$. We let $T = 1$ such that the interface remains easy to resolve.

The deformation field proposed by Leveque [18] is considered in 3D

$$\bar{\mathbf{u}}(t, \mathbf{x}) = \cos(\pi t/T) \begin{bmatrix} 2 \sin(\pi x)^2 \sin(2\pi y) \sin(2\pi z) \\ -\sin(2\pi x) \sin(\pi y)^2 \sin(2\pi z) \\ -\sin(2\pi x) \sin(2\pi y) \sin(\pi z)^2 \end{bmatrix},$$

where a sphere of radius $R = 0.15$ is initially located at $\mathbf{x}_0 = [0.35 \ 0.35 \ 0.35]^T$. The period is again taken as $T = 1$.

We will now explicitly denote an approximation to $\tilde{\varphi}$ as $\tilde{\tilde{\varphi}}$.

5.1. Comparison of the one- and two-velocity formulation

First we will compare the one- and two-velocity formulations in terms of the advection of the discontinuous field given by eq. (60). In figs. 12a and 12b we show the intermediate solutions of the 2D vortex reverse problem when using the LW flux interpolant with the two- and one-velocity formulation respectively. The LW flux results in the appearance of wiggles in the lighter gas phase when the one-velocity formulation is used, the two-velocity formulation however yields satisfactory results. Using the Fromm flux results in an absence of wiggles also in the one-velocity formulation, as shown in fig. 12c. Of course the shear layer is still diffuse, contrary to the sharp shear layer found with the two-velocity formulation.

These observations are reflected in fig. 13 where we show the accuracy of the advection method in terms of the L^1 -norm of the error at $t = T$, for each of the phases separately. We combine the results from the 2D vortex reverse as well as 3D deformation problem. Because the liquid phase is heavier, it is favoured by eq. (57), and therefore the accuracy in the liquid phase is the same for the two formulations, which is close to second-order. In the gas phase we however find that the one-velocity formulation results in less than first-order accuracy, whereas for the two-velocity formulation the accuracy is again of second-order.

5.2. Comparison of flux interpolants (2D)

We now consider the effect of the flux interpolant on the accuracy of the advection method, in 2D. To separate the effect of the CTU flux interpolant from the higher-order flux interpolants,

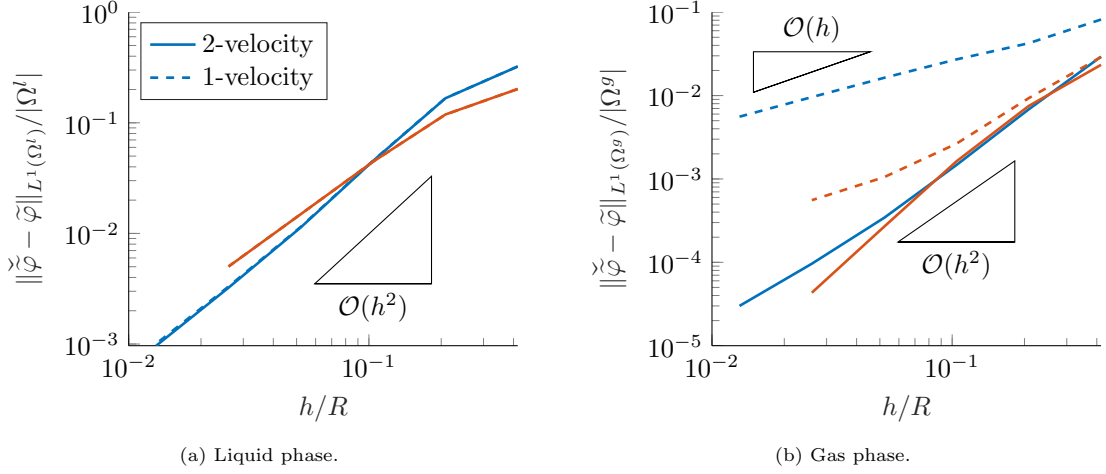


Figure 13: Comparison of the one- and two-velocity formulations in terms of the L^1 -norm of the error at $t = T$ for the 2D vortex reverse problem (blue) and 3D deformation problem (red). The Fromm flux was used.

we also consider a simulation without an interface ($\Omega^l = \Omega$). The accuracy in terms of the L^1 -norm, in the absence of an interface, is shown in fig. 14a. We find that the higher-order flux interpolants (excluding the upwind interpolant) are third-order accurate in space and time (the CFL constraint is fixed at $\nu^\dagger = \frac{1}{2}$, see also eq. (31)). In fig. 14b we show the accuracy in the presence of an interface, where the two-velocity formulation is used. We only show the accuracy of the liquid phase, as the accuracy in the gas phase was found to be similar. The results show that the flux interpolants, except for the upwind interpolant, are close to second-order accurate in the L^1 -norm and of very similar accuracy. Moreover we find that the error is two orders of magnitude larger than what we found in the absence of an interface, which suggests that the first-order error at the interface, due to the CTU flux interpolant, dominates the overall accuracy.

We furthermore consider how well quadratic invariants are conserved (see Appendix C), where we define the ‘kinetic energy’ of the passively advected scalar as

$$E_k^\pi := \frac{1}{2} \sum_{\omega(\mathcal{F})} \tilde{\alpha}^\pi \rho^\pi (\tilde{\varphi}^\pi)^2.$$

The change in kinetic energy is defined as

$$\Delta E_k^\pi(t) := E_k^\pi(t) - E_k^\pi(0).$$

The resulting change in kinetic energy at $t = T$, relative to the initial kinetic energy, is shown in figs. 15a and 15b for the simulation without and with the interface respectively. In the absence of an interface, we find that the higher-order methods are third-order accurate, where the LW flux interpolant yields the smallest change in kinetic energy, as can be expected from the discussion in Appendix C. When an interface is included, however, we find that significantly more energy is lost, which is attributed to the use of the first-order accurate CTU flux interpolant at the interface.

5.3. Effect of the parameters ν^\dagger and α^\dagger (2D)

Finally we consider the effect of the CFL limit ν^\dagger (see also eq. (31)) and the parameter α^\dagger (as required in eq. (55), see also lemma 3 and eq. (56)) on the accuracy as well as conservation of

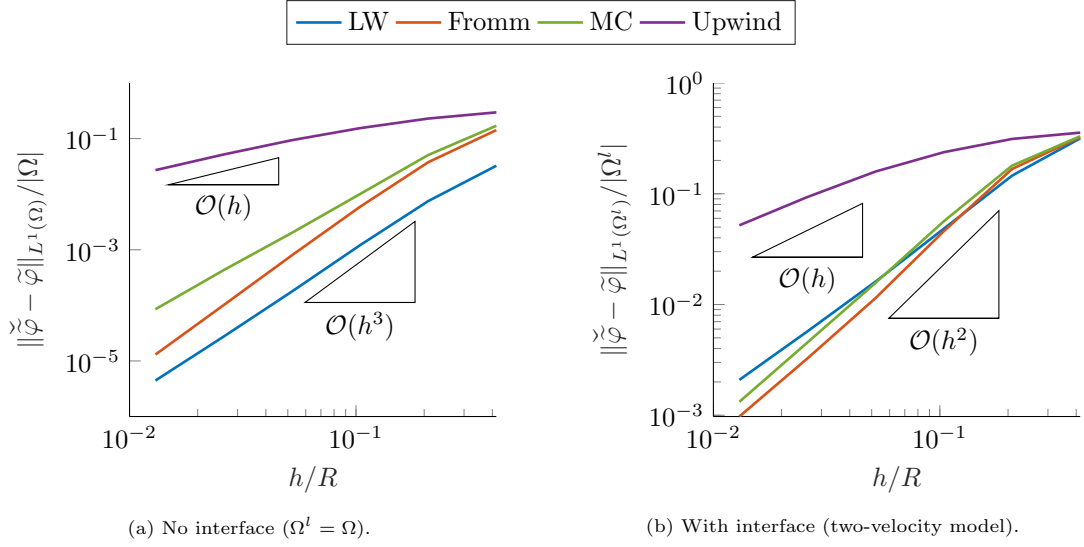


Figure 14: Comparison of the flux interpolants in terms of the L^1 -norm of the error at $t = T$ for the 2D vortex reverse problem.

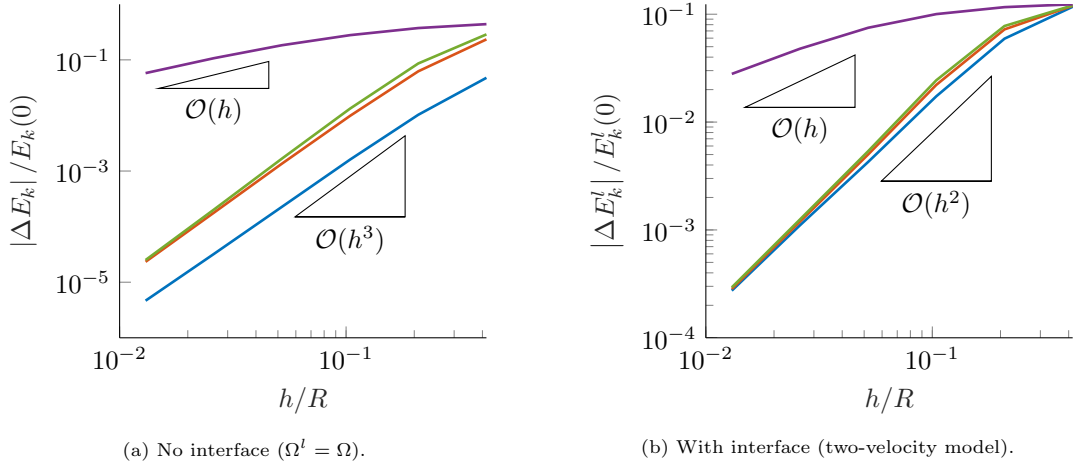


Figure 15: Comparison of the flux interpolants in terms of the loss of kinetic energy at $t = T$ for the 2D vortex reverse problem.

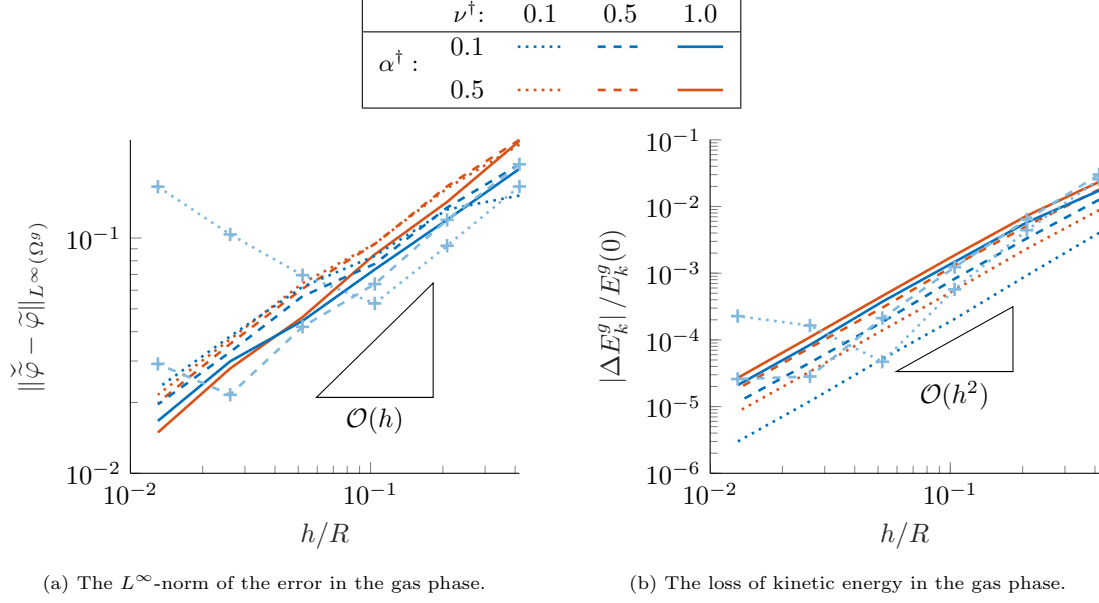


Figure 16: Comparison of the parameters ν^\dagger and α^\dagger for the 2D vortex reverse problem, using the LW flux interpolant. The markers (shown only for two pairs of $(\nu^\dagger, \alpha^\dagger)$) result from using the Fromm flux interpolant. The two-velocity formulation was used.

kinetic energy. Recall that the parameter α^\dagger determines when we use the CTU flux interpolant: if $\hat{\alpha}_f^{\pi, (n+1)} < \alpha^\dagger$ then the CTU flux interpolant is used on all faces of ω_f . As the parameter α^\dagger only has an influence at the interface, and results in the use of the first-order accurate CTU flux interpolant, we now consider the L^∞ -norm of the error at $t = T$ such that we essentially obtain the accuracy at the interface.

We consider mesh refinement for $\nu^\dagger \in \{0.1, 0.5, 1.0\}$ and $\alpha^\dagger \in \{0.1, 0.5\}$, as shown in fig. 16. In fig. 16a the resulting L^∞ -norm of the error in the gas phase is shown, where we made use of the LW flux interpolant (no markers) as well as the Fromm flux interpolant (markers, shown only for two pairs of $(\nu^\dagger, \alpha^\dagger)$). We find that varying the parameters hardly affects the accuracy at the interface when the LW flux interpolant is used. What little effect there is, consistently shows that taking larger time steps (i.e. considering larger values of ν^\dagger) yields a more accurate solution for a fixed value of α^\dagger . When the Fromm flux interpolant is used, we find that using $\alpha^\dagger = 0.1$ yields divergence of the solution under time step refinement (i.e. $\nu^\dagger \rightarrow 0$), suggesting that α^\dagger should not be taken too small when the Fromm flux interpolant is used. Note that we have shown the results using the Fromm flux interpolant only for those two pairs of $(\nu^\dagger, \alpha^\dagger)$ which yield divergence of the solution. Exactly why this occurs with the Fromm flux interpolant, and not with the LW flux interpolant, is unclear.

The loss in kinetic energy is shown in fig. 16b. A lower value of α^\dagger does lead to improved conservation of kinetic energy when the LW flux interpolant is used, as can be expected because the CTU flux interpolant is used less frequently. Moreover we find that taking a smaller time step, resulting in a smaller value of ν^\dagger , similarly leads to improved conservation of kinetic energy, as can be expected from the discussion in Appendix C.

This leads to the question of how much the conservation of kinetic energy can be improved by letting both ν^\dagger and α^\dagger tend to zero. Based on the upper bound given by eq. (56), where the ratio $\nu^\dagger/\alpha^\dagger$ appears, we now let $\alpha^\dagger = \nu^\dagger$ such that we use the CTU flux interpolant as little as possible,

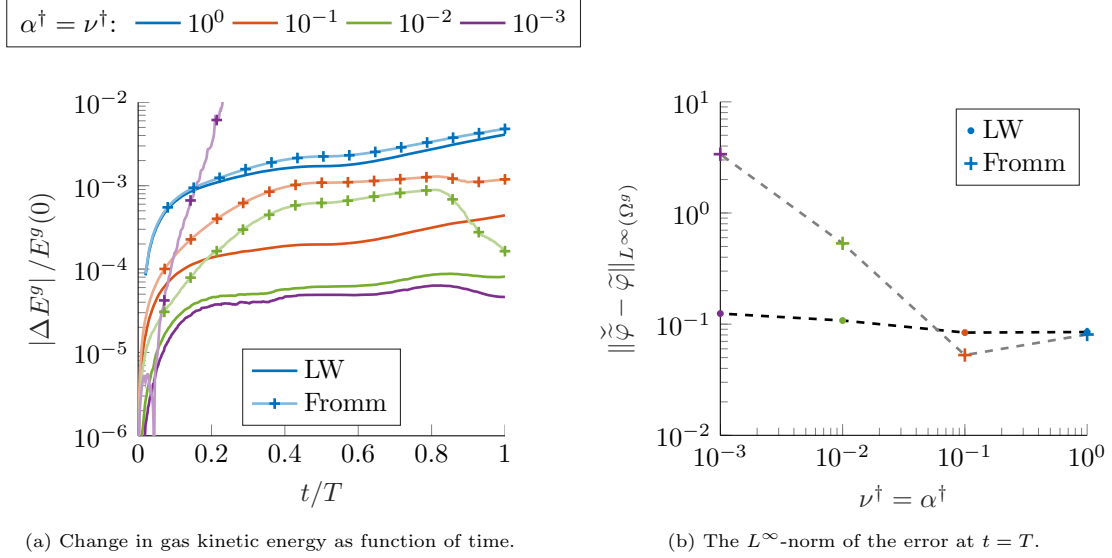


Figure 17: Reducing the time-step size ($\nu^\dagger \rightarrow 0$, where we let $\alpha^\dagger = \nu^\dagger$), for the 2D vortex reverse problem, where the mesh width is fixed and given by $h/R \approx 0.1$. We only show results from the gas phase, as results from the liquid phase show the same trends. The two-velocity formulation was used.

while still having boundedness of the solution. We let $h/R \approx 0.1$, and consider four different values of $\alpha^\dagger = \nu^\dagger \in \{10^0, 10^{-1}, 10^{-2}, 10^{-3}\}$. The resulting evolution of kinetic energy in the gas phase is shown in fig. 17a, where we consider both the LW and Fromm flux interpolant. For the LW flux interpolant we initially find a significant improvement in the conservation of kinetic energy when decreasing the value of $\alpha^\dagger = \nu^\dagger$. Hence even though we use the *modified* LW flux interpolant, which uses the dissipative CTU flux interpolant (which does not satisfy eq. (C.3)) at the interface, the analysis presented in Appendix C still holds in some sense when $\alpha^\dagger = \nu^\dagger \rightarrow 0$. On the other hand, the Fromm flux interpolant does not yield much of an improvement in the conservation of kinetic energy and moreover yields divergence of the solution, as is illustrated in fig. 17b. It's unclear why the Fromm flux interpolant leads to divergence of the solution when $\alpha^\dagger = \nu^\dagger \rightarrow 0$.

6. Discussion

In an effort to model the shear layer at the interface, we have proposed the use of a two-velocity formulation of the two-phase Navier–Stokes equations. For now we have focussed our attention on the transport of mass and momentum in such a two-velocity formulation.

To conserve mass and momentum in a sharp and accurate way, we follow the approach originally proposed in Rudman [30] and use the same approximate space-time integration of the advection equation for momentum as is used for the advection of mass. The dimensionally unsplit advection method used for the transport of mass and momentum relies on the construction of donating regions. We have derived sufficient conditions on these donating regions which ensure boundedness of the resulting volume fraction (corollary 1).

For the advection of a staggered momentum field we propose a simple averaging of the same mass fluxes that are used for advecting the centred mass. For our proposed one- and two-velocity formulations this implies that, besides the conservation of mass, the total and liquid linear momentum respectively are conserved exactly, without the need for computing additional

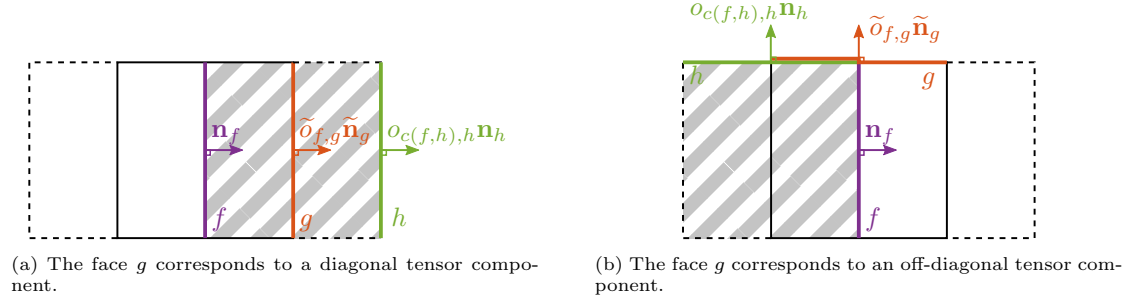


Figure A.1: We can uniquely identify a centred control volume $c(f, h) \in \mathcal{C}(f)$ to the pair f, h , provided that $g \in \mathcal{G}(\omega_f)$, $h \in \mathcal{F}(g)$ and $f \neq h$. The faces f, h both belong to the boundary of the hatched centred control volume $c(f, h)$ and therefore $f, h \in \mathcal{F}(c(f, h))$.

mass fluxes. We find that such an interpolation yields a direct relation between the centred and staggered advection methods (as given by eq. (49)). Furthermore we show that the advection method in semi-discrete form conserves quadratic invariants (i.e. kinetic energy), provided that the Lax–Wendroff flux interpolant is used.

The velocity (per phase) can be computed by dividing the momentum with the corresponding mass, however such a division is not always well-defined if the corresponding mass nearly vanishes during a single time step. We have introduced a modified flux interpolant for which we can guarantee that the division is well defined, under the condition that the donating regions are absent of any flux overlap and transit errors (lemmas 2 and 3).

The proposed methods are shown to converge under mesh refinement for two- and three-dimensional reversible deformation test cases. The passive transport of a discontinuous scalar shows that the one-velocity formulation yields low accuracy for the lighter of the two phases. This is because the advection of the velocity field in the one-velocity formulation favours the heavier liquid phase. To the contrary, using the two-velocity formulation results in the same accuracy for both phases, regardless of the density ratio.

In a future paper we will focus our attention on coupling the two phases in the Navier–Stokes equations via a novel jump condition that is included in the pressure Poisson problem. For future work it would moreover be interesting to see if a less dissipative flux interpolant can be constructed at the interface, resulting in second-order accuracy in the L^∞ -norm, while still guaranteeing boundedness. The proposed methods are compatible with adaptive mesh refinement (AMR). The restriction and prolongation operators between the refinement levels are however not yet momentum conservative, and it would therefore be interesting to develop this and obtain exact momentum conservation also when AMR is used.

Acknowledgements

This work is part of the research programme SLING, which is (partly) financed by the Netherlands Organisation for Scientific Research (NWO). We would like to thank the Center for Information Technology of the University of Groningen for their support and for providing access to the Peregrine high performance computing cluster. Moreover we thank Dr. Joaquín López (Universidad Politécnica de Cartagena) for kindly providing the VoFTools library.

Appendix A. Operator connection

Lemma 1 (Operator connection). *For the previously introduced operators eqs. (4) and (6) to (8) it holds that*

$$\tilde{\mathfrak{D}}\tilde{\mathfrak{I}} = \mathfrak{I}\mathfrak{D}. \quad (9)$$

Proof. We start by applying the left-hand side of eq. (9) to some field $m \in \mathcal{F}^h$

$$|\omega_f|(\tilde{\mathfrak{D}}\tilde{\mathfrak{I}}m)_f = \frac{1}{2} \sum_{g \in \mathcal{G}(\omega_f)} \sum_{h \in \mathcal{F}(g)} \tilde{o}_{f,g}(\tilde{\mathbf{n}}_g \cdot \mathbf{n}_h) |h| m_h, \quad (A.1)$$

where we have substituted eqs. (7) and (8). The union over the faces $\mathcal{F}(g)$, for all faces $g \in \mathcal{G}(\omega_f)$, is the same as the union over the faces $\mathcal{F}(c)$, for all control volumes $c \in \mathcal{C}(f)$ (see also fig. 5a)

$$\bigcup_{g \in \mathcal{G}(\omega_f)} \mathcal{F}(g) = \bigcup_{c \in \mathcal{C}(f)} \mathcal{F}(c). \quad (A.2)$$

This identity can be exploited to rewrite the double summation in eq. (A.1), but in doing so we must get rid of the dependence on $g \in \mathcal{G}(\omega_f)$ in the $\tilde{o}_{f,g}(\tilde{\mathbf{n}}_g \cdot \mathbf{n}_h)$ term, and instead express it in terms of $c \in \mathcal{C}(f)$.

In order to do so, we uniquely identify a centred control volume to the pair f, h , which we denote by $c(f, h)$, and for which it holds that $f, h \in \mathcal{F}(c(f, h))$, see also fig. A.1. Provided that $f \neq h$, it holds that the outward pointing normal of the staggered control volume $\tilde{\omega}_f$ coincides with the outward pointing normal of the centred control volume $c \in \mathcal{C}(f)$

$$\tilde{o}_{f,g}\tilde{\mathbf{n}}_g = o_{c(f,h),h}\mathbf{n}_h \implies \tilde{o}_{f,g}(\tilde{\mathbf{n}}_g \cdot \mathbf{n}_h) = o_{c(f,h),h}, \quad (A.3)$$

as illustrated in fig. A.1. Note that the two contributions in eq. (A.1) for $f = h$ cancel, and therefore it does not matter that the above identity only holds for $f \neq h$. Substitution of eq. (A.3) into eq. (A.1), and subsequently utilising eq. (A.2), results in

$$|\omega_f|(\tilde{\mathfrak{D}}\tilde{\mathfrak{I}}m)_f = \frac{1}{2} \sum_{g \in \mathcal{G}(\omega_f)} \sum_{h \in \mathcal{F}(g)} o_{c(f,h),h} |h| m_h \stackrel{(A.2)}{=} \frac{1}{2} \sum_{c \in \mathcal{C}(f)} \sum_{h \in \mathcal{F}(c)} o_{c,h} |h| m_h = |\omega_f|(\mathfrak{I}\mathfrak{D}m)_f, \quad (A.4)$$

where we have used the definition of the divergence and interpolation operator given by eqs. (4) and (6). Equation (A.4) holds for any $m \in \mathcal{F}^h$ and therefore we find that eq. (9) indeed holds true. \square

Appendix B. Analysis of DR methods

Theorem 1 (Bounded outflow). *The outgoing flow is bounded by the π -phase volume fraction contained in the control volume c at $t = t^{(n)}$*

$$V^{-,\pi} \leq \alpha^{\pi,(n)}, \quad (26)$$

provided that the approximate DRs do not contain any flux overlap nor transit errors.

Proof. We will omit the superscript (n) . Substitution of the definition of the partial volume fluxes eq. (19) into the definition of the outgoing volume eq. (25) results in

$$|c|V_c^{-,\pi} = - \sum_{b \in \mathcal{C}(c)} \left[- \sum_{f \in \mathcal{F}(c)} o_{c,f} M_0(b \cap \Omega^\pi \cap \bar{\Delta}_f) \right]^{-},$$

where we recall that $b^\pi = b \cap \Omega^\pi$. By making use of the notation of scalar multiplication, as defined in eq. (15), of an oriented DR (where the scalar must be plus or minus one), we can move the multiplication by $-o_{c,f}$ inside $M_0(\dots)$ to the oriented set $\bar{\Delta}_f$, resulting in

$$|c|V_c^{-,\pi} = - \sum_{b \in \mathcal{C}(c)} \left[\sum_{f \in \mathcal{F}(c)} M_0(b \cap \Omega^\pi \cap (-o_{c,f} \bar{\Delta}_f)) \right]^-.$$

Note that an absence of flux overlap errors (see eq. (20)) implies that the summation over the faces of the volumes can equivalently be written as the volume of the union of the sets, that is

$$|c|V_c^{-,\pi} = - \sum_{b \in \mathcal{C}(c)} [M_0(b \cap \Omega^\pi \cap \bar{\Delta}_c)]^- \quad (\text{B.1})$$

where we have defined the oriented union of the DRs as

$$\bar{\Delta}_c := \bigcup_{f \in \mathcal{F}(c)} -o_{c,f} \bar{\Delta}_f. \quad (\text{B.2})$$

For any two non-oriented sets A, B it holds that A can be written as the union of the following two non-overlapping sets: $A = (A \setminus B) \cup (A \cap B)$. The definition of our oriented set allows for a similar result

$$\bar{\Delta}_c = (\bar{\Delta}_c \setminus -\bar{\Delta}_c) \cup (\bar{\Delta}_c \cap -\bar{\Delta}_c), \quad (\text{B.3})$$

where $\bar{\Delta}_c \cap -\bar{\Delta}_c$ results from overlapping DRs with opposite relative orientation, resulting in the phase volume that is merely in transit as shown by the hatched regions in fig. 2. Moreover, the intersection volume of any non-oriented set A with the second bracketed term in the right-hand side of eq. (B.3) vanishes

$$M_0(A \cap (\bar{\Delta}_c \cap -\bar{\Delta}_c)) = |A \cap (\bar{\Delta}_c^+ \cap \bar{\Delta}_c^-)| - |A \cap (\bar{\Delta}_c^- \cap \bar{\Delta}_c^+)| = 0, \quad (\text{B.4})$$

which follows from eqs. (14) and (15), and reflects the fact that fluid that is merely in transit does not contribute to the change in volume within the control volume c .

The two bracketed sets in eq. (B.3) are non-overlapping and therefore the outgoing volume can be written as

$$\begin{aligned} |c|V_c^{-,\pi} &= - \sum_{b \in \mathcal{C}(c)} [M_0(b \cap \Omega^\pi \cap (\bar{\Delta}_c \setminus -\bar{\Delta}_c))]^- \\ &= - \sum_{b \in \mathcal{C}(c)} [|b \cap \Omega^\pi \cap (\bar{\Delta}_c^+ \setminus \bar{\Delta}_c^-)| - |b \cap \Omega^\pi \cap (\bar{\Delta}_c^- \setminus \bar{\Delta}_c^+)|]^- , \end{aligned} \quad (\text{B.5})$$

where we made use of eqs. (14), (B.1), (B.3) and (B.4). Recall from section 3.1 that the orientation of a part of the DR $\bar{\Delta}_f$ is defined as negative if the face normal \mathbf{n}_f points into it, and therefore the positively orientated part $\bar{\Delta}_c^+$ of the oriented union of the DRs, as given by eq. (B.2), lies outside of c : $\bar{\Delta}_c^+ \cap c = \emptyset$. From this observation it follows that $b \cap \bar{\Delta}_c^+ \setminus \bar{\Delta}_c^- = \emptyset$ if $b = c$ and moreover assuming an absence of flux transit errors (see eq. (21)) implies that $b \cap \bar{\Delta}_c^- \setminus \bar{\Delta}_c^+ = \emptyset$ if $b \neq c$. It follows that eq. (B.5) can be written as

$$|c|V_c^{-,\pi} = - \sum_{b \in \mathcal{C}(c) \setminus c} [|b \cap \Omega^\pi \cap (\bar{\Delta}_c^+ \setminus \bar{\Delta}_c^-)|]^- - [-|c \cap \Omega^\pi \cap (\bar{\Delta}_c^- \setminus \bar{\Delta}_c^+)|]^- = |c \cap \Omega^\pi \cap (\bar{\Delta}_c^- \setminus \bar{\Delta}_c^+)|,$$

and therefore

$$|c|V_c^{-,\pi} \leq |c \cap \Omega^\pi| = |c| \alpha_c^\pi,$$

which coincides with the bounded outflow condition eq. (26). \square

Lemma 2 (Boundedness of the CTU flux interpolant). *The CTU flux interpolant eq. (53) results in boundedness of $\tilde{\varphi}^{\pi,(n+1)}$ in the following sense*

$$\left| \tilde{\varphi}_f^{\pi,(n+1)} - \tilde{\varphi}_f^{\pi,(n)} \right| \leq \max_{k \in \mathcal{F}(f)} \left| \tilde{\varphi}_k^{\pi,(n)} - \tilde{\varphi}_f^{\pi,(n)} \right|,$$

provided that the approximate DRs do not contain any flux overlap nor transit errors, and that the CFL constraint given by eq. (31) is satisfied for $\nu^\dagger \leq 1$.

Proof. We substitute $\tilde{\alpha}^{\pi,(n)} = \tilde{\alpha}^{\pi,(n+1)} + \delta t \tilde{\mathfrak{D}} \tilde{v}^{\pi,(n)}$ (as follows from eqs. (34), (47), (48) and (54) with $\tilde{\varphi} \equiv 1$) into eq. (50) and divide out the constant density ρ^π which appears in both the numerator and denominator, this results in

$$\tilde{\varphi}^{\pi,(n+1)} = \tilde{\varphi}^{\pi,(n)} + \delta t \frac{(\tilde{\mathfrak{D}} \tilde{v}^{\pi,(n)}) \tilde{\varphi}^{\pi,(n)} - \tilde{\mathfrak{D}}(\tilde{v}^{\pi,(n)}) \tilde{\mathfrak{F}}^{\text{CTU}} \tilde{\varphi}^{\pi,(n)}}{\tilde{\alpha}^{\pi,(n+1)}},$$

where we have made use of eq. (48) with $\tilde{\mathfrak{F}} = \tilde{\mathfrak{F}}^{\text{CTU}}$. Subsequently we combine both terms in the numerator (recall that the staggered divergence operator $\tilde{\mathfrak{D}}$ is given by eq. (7))

$$\tilde{\varphi}_f^{\pi,(n+1)} = \tilde{\varphi}_f^{\pi,(n)} + \delta t \frac{\sum_{g \in \mathcal{G}(\omega_f)} \tilde{o}_{f,g} |g| \tilde{v}_g^{\pi,(n)} \left(\tilde{\varphi}_f^{\pi,(n)} - (\tilde{\mathfrak{F}}^{\text{CTU}} \tilde{\varphi}^{\pi,(n)})_g \right)}{|\omega_f| \tilde{\alpha}_f^{\pi,(n+1)}},$$

and substitute the definition of the CTU flux interpolant eq. (53)

$$\tilde{\varphi}_f^{\pi,(n+1)} = \tilde{\varphi}_f^{\pi,(n)} + \delta t \frac{\sum_{k \in \mathcal{F}(f)} \sum_{g \in \mathcal{G}(\omega_f)} \tilde{o}_{f,g} |g| \tilde{v}_{g,k}^{\pi,(n)} \left(\tilde{\varphi}_f^{\pi,(n)} - \tilde{\varphi}_k^{\pi,(n)} \right)}{|\omega_f| \tilde{\alpha}_f^{\pi,(n+1)}}, \quad (\text{B.6})$$

where we have swapped the order of summation. We now split the term in the numerator of eq. (B.6) into the parts corresponding to the in- and outgoing flow

$$\frac{\tilde{\varphi}_f^{\pi,(n+1)} - \tilde{\varphi}_f^{\pi,(n)}}{\delta t} = \frac{N_f^{+,\pi} - N_f^{-,\pi}}{\tilde{\alpha}_f^{\pi,(n+1)}}, \quad (\text{B.7})$$

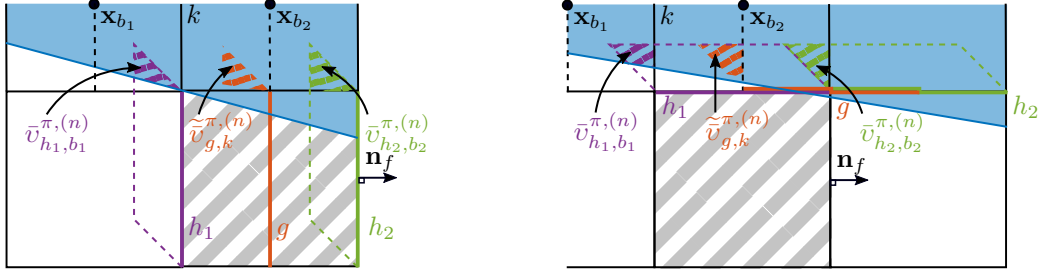
where the terms in the numerator are given by

$$N_f^{\pm,\pi} := \pm \frac{1}{|\omega_f|} \sum_{k \in \mathcal{F}(f)} \underbrace{\left[- \sum_{g \in \mathcal{G}(\omega_f)} \tilde{o}_{f,g} |g| \tilde{v}_{g,k}^{\pi,(n)} \right]}_{\text{fluid that flows out of } \omega_f \text{ (-), or from } \omega_k \text{ into } \omega_f \text{ (+)}} \left(\tilde{\varphi}_k^{\pi,(n)} - \tilde{\varphi}_f^{\pi,(n)} \right), \quad (\text{B.8})$$

corresponding to an outflow of $\tilde{\varphi}^{\pi,(n)}$ given by $N_f^{-,\pi}$, and an inflow into ω_f given by $N_f^{+,\pi}$. Note that swapping the order of summation in eq. (B.6), combined with the placement of $[\dots]^\pm$ in eq. (B.8), exactly results in the cancellation of any fluxes resulting from neighbouring DRs which are overlapping with an opposite relative orientation. This step is essential in being able to separately bound each of the terms in the numerator of eq. (B.7), and explicitly relies on the use of the partial volume fluxes.

For the remainder we need an explicit definition of the interpolated partial volume flux eq. (19), as illustrated in fig. B.2 and given by (cf. eqs. (8) and (54))

$$|g| \tilde{v}_{g,k}^{\pi,(n)} := \frac{1}{2} \sum_{h \in \mathcal{F}(g)} (\tilde{\mathbf{n}}_g \cdot \mathbf{n}_h) |h| \tilde{v}_{h,b(g,h,k)}^{\pi,(n)}, \quad (\text{B.9})$$



(a) The face g corresponds to a diagonal tensor component. Here $f = h_2$.

(b) The face g corresponds to an off-diagonal tensor component.

Figure B.2: Illustration of the interpolated partial volume flux as defined in eq. (B.9). The centred control volumes (solid lines) b_i are positioned the same, relative to faces h_i , as the staggered control volume ω_k is positioned relative to g . In this example we find $b_i = \hat{b}(g, h_i, k) \in \mathcal{C}(k)$. The gray hatched region corresponds to the control volume c , where, for example, $b_1 = b(c, f, k)$: b_1 is a diagonal neighbour of c in the same way that ω_k is a diagonal neighbour of ω_f .

where the centred control volume $\hat{b}(g, h, k) \in \mathcal{C}(k)$ is as illustrated in fig. B.2 and is positioned relative to h in the same way as ω_k is positioned relative to g . Using this definition of the interpolated partial volume flux we can write eq. (B.8) as

$$\begin{aligned}
 N_f^{\pm, \pi} &= \frac{\pm 1}{2|\omega_f|} \sum_{k \in \mathcal{F}(f)} \left[- \sum_{g \in \mathcal{G}(\omega_f)} \sum_{h \in \mathcal{F}(g)} \tilde{o}_{f,g}(\tilde{\mathbf{n}}_g \cdot \mathbf{n}_h) |h| \bar{v}_{h, \hat{b}(g, h, k)}^{\pi, (n)} \right]^{\pm} \left(\tilde{\varphi}_k^{\pi, (n)} - \tilde{\varphi}_f^{\pi, (n)} \right) \\
 &= \frac{\pm 1}{2|\omega_f|} \sum_{k \in \mathcal{F}(f)} \left[- \sum_{c \in \mathcal{C}(f)} \sum_{h \in \mathcal{F}(c)} o_{c,h} |h| \bar{v}_{h, b(c, f, k)}^{\pi, (n)} \right]^{\pm} \left(\tilde{\varphi}_k^{\pi, (n)} - \tilde{\varphi}_f^{\pi, (n)} \right), \quad (\text{B.10})
 \end{aligned}$$

where we have furthermore utilised eqs. (A.2) and (A.3) and have expressed $\hat{b}(g, h, k)$ as $b(c, f, k)$. That is, ω_k is a neighbour of ω_f in the same way that $b(c, f, k)$ is a neighbour of c , see also fig. B.2.

We will now first show that the outflow term vanishes identically: $N_f^{-, \pi} = 0$. The arguments used are identical to those used in the proof of theorem 1. Substitution of the definition of the partial volume flux given by eq. (19) into eq. (B.10) results in

$$N_f^{-, \pi} = -\frac{1}{2\delta t |\omega_f|} \sum_{k \in \mathcal{F}(f)} \left[- \sum_{c \in \mathcal{C}(f)} \sum_{h \in \mathcal{F}(c)} o_{c,h} M_0(\bar{\Delta}_h^{(n)} \cap b(c, f, k)^{\pi, (n)}) \right]^{-} \left(\tilde{\varphi}_k^{\pi, (n)} - \tilde{\varphi}_f^{\pi, (n)} \right).$$

We then move the multiplication by the orientation $-o_{c,h}$ into the signed volume, and moreover make use of the assumption that neighbouring DRs do not overlap, which permits replacing the summation over $h \in \mathcal{F}(c)$ with a union of the DRs (as defined in eq. (B.2)), resulting in

$$N_f^{-, \pi} = -\frac{1}{2\delta t |\omega_f|} \sum_{k \in \mathcal{F}(f)} \left[\sum_{c \in \mathcal{C}(f)} M_0(\bar{\Delta}_c^{(n)} \cap b(c, f, k)^{\pi, (n)}) \right]^{-} \left(\tilde{\varphi}_k^{\pi, (n)} - \tilde{\varphi}_f^{\pi, (n)} \right).$$

Subsequently we make use of eqs. (B.3) and (B.4), from which it follows that the outflow term

can be written as

$$N_f^{-,\pi} = -\frac{1}{2\delta t|\omega_f|} \sum_{k \in \mathcal{F}(f)} \left[\sum_{c \in \mathcal{C}(f)} M_0(b(c, f, k)^{\pi, (n)} \cap (\bar{\Delta}_c^{(n)} \setminus -\bar{\Delta}_c^{(n)})) \right]^- \left(\tilde{\varphi}_k^{\pi, (n)} - \tilde{\varphi}_f^{\pi, (n)} \right). \quad (\text{B.11})$$

Note that only $k \neq f$ will contribute to eq. (B.11), and therefore by the definition of $b(c, f, k)$ we can assume $b(c, f, k) \neq c$.

Recall that $\bar{\Delta}_c^{(n)}$ is an oriented DR, and therefore

$$M_0(b^\pi \cap (\bar{\Delta}_c^{(n)} \setminus -\bar{\Delta}_c^{(n)})) \stackrel{(14)}{=} \left| b^\pi \cap (\bar{\Delta}_c^{+, (n)} \setminus \bar{\Delta}_c^{-, (n)}) \right| - \left| b^\pi \cap (\bar{\Delta}_c^{-, (n)} \setminus \bar{\Delta}_c^{+, (n)}) \right|, \quad (\text{B.12})$$

where we note that $\bar{\Delta}_c^{-, (n)} \setminus \bar{\Delta}_c^{+, (n)} \cap b = \emptyset$ if $b \neq c$, thanks to an absence of flux transit errors. This implies that (B.12) can be written as (assuming $b \neq c$)

$$M_0(b^\pi \cap (\bar{\Delta}_c^{(n)} \setminus -\bar{\Delta}_c^{(n)})) = \left| b^\pi \cap (\bar{\Delta}_c^{+, (n)} \setminus \bar{\Delta}_c^{-, (n)}) \right|.$$

This result can be used to write eq. (B.11) as

$$N_f^{-,\pi} = -\frac{1}{2\delta t|\omega_f|} \sum_{k \in \mathcal{F}(f)} \left[\sum_{c \in \mathcal{C}(f)} \left| b(c, f, k)^{\pi, (n)} \cap (\bar{\Delta}_c^{+, (n)} \setminus \bar{\Delta}_c^{-, (n)}) \right| \right]^- \left(\tilde{\varphi}_k^{\pi, (n)} - \tilde{\varphi}_f^{\pi, (n)} \right) = 0, \quad (\text{B.13})$$

where we made use of $[x]^- = 0$ if $x \geq 0$. Hence thanks to an assumed absence of flux overlap and transit errors, as well as the use of the CTU flux interpolant, we can guarantee that the outflow $N_f^{-,\pi}$ does not affect the change in $\tilde{\varphi}_f^\pi$ in eq. (B.7).

The inflow, which was the first term in the numerator of the right-hand side of eq. (B.7), can be bounded in the following way

$$|N_f^{+,\pi}| \leq \frac{\tilde{V}_f^{+,\pi}}{\delta t} \max_{k \in \mathcal{F}(f)} \left| \tilde{\varphi}_k^{\pi, (n)} - \tilde{\varphi}_f^{\pi, (n)} \right|, \quad (\text{B.14})$$

where we made use of eq. (B.10) and we define the staggered ingoing flow (cf. eq. (25)) as

$$\tilde{V}_f^{+,\pi} := \frac{\delta t}{2|\omega_f|} \sum_{k \in \mathcal{F}} \left[- \sum_{c \in \mathcal{C}(f)} \sum_{h \in \mathcal{F}(c)} o_{c,h} |h| \bar{v}_{h, b(c, f, k)}^{\pi, (n)} \right]^+. \quad (\text{B.15})$$

In eq. (B.15) we have replaced the summation over $k \in \mathcal{F}(f)$ (summing over the neighbours of ω_f) by a summation over $k \in \mathcal{F}$ (assuming a CFL constraint there will be no contributions from $\mathcal{F} \setminus \mathcal{F}(f)$). We now note that summing over all $k \in \mathcal{F}$ results in all centred control volumes $b(c, f, k)$ to be considered, which implies that the staggered ingoing flow can equivalently be written as

$$\tilde{V}_f^{+,\pi} := \frac{\delta t}{2|\omega_f|} \sum_{b \in \mathcal{C}} \left[- \sum_{c \in \mathcal{C}(f)} \sum_{h \in \mathcal{F}(c)} o_{c,h} |h| \bar{v}_{h, b}^{\pi, (n)} \right]^+.$$

The staggered ingoing flow can now be bounded in the following way

$$\tilde{V}_f^{+, \pi} \leq \frac{\delta t}{2|\omega_f|} \sum_{c \in \mathcal{C}(f)} \sum_{b \in \mathcal{C}} \left[- \sum_{h \in \mathcal{F}(c)} o_{c,h} |h| \bar{v}_{h,b}^{\pi, (n)} \right]^+ \stackrel{(25)}{=} (\mathfrak{I}V^{+, \pi})_f, \quad (\text{B.16})$$

where we have used the algebraic identity $[a_1 + a_2 + \dots]^+ \leq [a_1]^+ + [a_2]^+ + \dots$ and finally have substituted the definition of the centred outgoing volume eq. (25) as well as the interpolant given by eq. (6).

Since we have assumed that the DRs do not commit any flux overlap nor transit errors, we may use the result of theorem 1 which implies that the interpolated ingoing volume flow is bounded by the staggered volume fraction at $t = t^{(n+1)}$

$$\mathfrak{I}V^{+, \pi} \stackrel{(24)}{=} \mathfrak{I} \left[\alpha^{\pi, (n+1)} - (\alpha^{\pi, (n)} - V^{-, \pi}) \right] \leq \mathfrak{I} \alpha^{\pi, (n+1)} = \tilde{\alpha}^{\pi, (n+1)}. \quad (\text{B.17})$$

Combining the results of eqs. (B.7), (B.13), (B.14), (B.16) and (B.17) then concludes the proof. \square

Lemma 3 (Boundedness of the modified flux interpolant). *Assuming that $\tilde{\alpha}_f^{\pi, (n+1)} \geq \alpha^\dagger$, we find that the temporal update in $\tilde{\varphi}^\pi$ is bounded in the following sense*

$$\left| \tilde{\varphi}_f^{\pi, (n+1)} - \tilde{\varphi}_f^{\pi, (n)} \right| \leq \frac{\tilde{W}_f^{+, \pi} + \tilde{W}_f^{-, \pi}}{\alpha^\dagger} \max_{g \in \mathcal{G}(\omega_f)} \left| (\tilde{\mathfrak{F}}^{\text{Method}^*} \tilde{\varphi}^{\pi, (n)})_g - \tilde{\varphi}_f^{\pi, (n)} \right|,$$

where the in- and outgoing volume, without re-ordering the summation over the partial volume fluxes, is given by

$$\tilde{W}_f^{\pm, \pi} := \pm \frac{\delta t}{|\omega_f|} \sum_{g \in \mathcal{G}(\omega_f)} \left[-\tilde{o}_{f,g} |g| \tilde{v}_g^{\pi, (n)} \right]^\pm.$$

Proof. As with the proof of lemma 2, we can write eq. (47) as (cf. eq. (B.7))

$$\frac{\tilde{\varphi}_f^{\pi, (n+1)} - \tilde{\varphi}_f^{\pi, (n)}}{\delta t} = \frac{M_f^{+, \pi} - M_f^{-, \pi}}{\tilde{\alpha}_f^{\pi, (n+1)}} \quad (\text{B.18})$$

where the terms in the numerator are defined as (cf. eq. (B.8))

$$M_f^{\pm, \pi} := \pm \frac{1}{|\omega_f|} \sum_{g \in \mathcal{G}(\omega_f)} \left[-\tilde{o}_{f,g} |g| \tilde{v}_g^{\pi, (n)} \right]^\pm \left((\tilde{\mathfrak{F}}^{\text{Method}^*} \tilde{\varphi}^{\pi, (n)})_g - \tilde{\varphi}_f^{\pi, (n)} \right).$$

Each of the terms in the numerator of the right-hand side of eq. (B.18) can be bounded as follows

$$\left| M_f^{\pm, \pi} \right| \leq \frac{\tilde{W}_f^{\pm, \pi}}{\delta t} \max_{g \in \mathcal{G}(\omega_f)} \left| (\tilde{\mathfrak{F}}^{\text{Method}^*} \tilde{\varphi}^{\pi, (n)})_g - \tilde{\varphi}_f^{\pi, (n)} \right|. \quad (\text{B.19})$$

Combining eqs. (B.18) and (B.19) as well as the assumption $\tilde{\alpha}_f^{\pi, (n+1)} \geq \alpha^\dagger$ then yields the desired result. \square

Appendix C. Semi-discrete conservation of quadratic invariants

We will use the following short-hand notation for discrete integration

$$\sum_{\omega(\mathcal{F})} \tilde{\varphi} := \sum_{f \in \mathcal{F}} |\omega_f| \tilde{\varphi}_f, \quad \sum_{\mathcal{G}} T := \sum_{g \in \mathcal{G}} |\tilde{\omega}_g| T_g. \quad (\text{C.1})$$

Whenever we refer to the adjoint of an operator, e.g. \mathfrak{D}^T , the use of the L^2 inner product induced by the previously defined integral functionals in eq. (C.1) is implied. We consider the one-velocity formulation.

Conservation of quadratic invariants is usually studied in semi-discrete form [36, 38]. Our discretisation of eq. (3) is however based on approximate space-time integration, resulting in eq. (47), and we therefore initially do not have a semi-discrete equation to study. We can however take the limit $\delta t \rightarrow 0$ of eq. (47), and obtain a semi-discretisation via that way. In this limit the volume flux can be written as

$$\lim_{\delta t \rightarrow 0} \bar{v}^{\pi, (n)} = a^{\pi, (n)} \bar{u}^{(n)},$$

and therefore the space-time integration approach discussed in section 4, resulting in eq. (47), can be viewed as a specialised time integration of the following semi-discretisation

$$\frac{d}{dt} (\tilde{\alpha} \rho \tilde{\varphi})^\pi + \tilde{\mathfrak{A}}[\bar{m}^\pi] \tilde{\varphi}^\pi = 0, \quad (\text{C.2})$$

where the mass flux is now given by

$$\bar{m}^\pi = \rho^\pi a^\pi \bar{u}.$$

Moreover, in the same limit we find that the LW flux interpolant eq. (51) reduces to a central spatial discretisation (see fig. 11, in this limit the centroid of the DR coincides with the face centroid, and therefore $\tilde{\mathfrak{U}}_1 \tilde{\varphi}$ will coincide with the upwind centred value of $\tilde{\varphi}$)

$$\lim_{\delta t \rightarrow 0} \tilde{\mathfrak{F}}^{\text{LW}} \tilde{\varphi} = \frac{1}{2} \tilde{\mathfrak{U}}_0 \tilde{\varphi} + \frac{1}{2} \tilde{\mathfrak{U}}_1 \tilde{\varphi} = \tilde{\mathfrak{E}} \tilde{\varphi}, \quad (\text{C.3})$$

where the equal weight interpolant $\tilde{\mathfrak{E}} : \mathcal{F}^h \rightarrow \mathcal{G}^h$ is defined as

$$(\tilde{\mathfrak{E}} \tilde{\varphi})_g := \frac{1}{2} \sum_{f \in \mathcal{F}^\omega(g)} \tilde{\varphi}_f.$$

We will now show that the semi-discretisation eq. (C.2) conserves kinetic energy if the LW interpolant is used. For ease of notation we will omit the superscript π on α, ρ, φ and \bar{m} . The temporal evolution of the kinetic energy density is given by

$$\frac{1}{2} \frac{d}{dt} (\rho \tilde{\alpha} \tilde{\varphi}^2) = \frac{1}{2} \frac{d}{dt} \left[\frac{(\rho \tilde{\alpha} \tilde{\varphi})^2}{\rho \tilde{\alpha}} \right] = \tilde{\varphi} \frac{d}{dt} (\rho \tilde{\alpha} \tilde{\varphi}) - \frac{1}{2} \tilde{\varphi}^2 \frac{d}{dt} (\rho \tilde{\alpha}) = -\tilde{\varphi} \tilde{\mathfrak{A}}[\bar{m}] \tilde{\varphi} + \frac{1}{2} \tilde{\varphi}^2 \tilde{\mathfrak{A}}[\bar{m}] 1, \quad (\text{C.4})$$

where we have used the quotient rule, product rule as well as eq. (C.2) and again eq. (C.2) with $\tilde{\varphi} = 1$.

Integration of the first term that appears in the operator in the right-hand side of eq. (C.4) results in

$$-\sum_{\omega(\mathcal{F})} \tilde{\varphi} \tilde{\mathfrak{A}}[\bar{m}] \tilde{\varphi} = -\sum_{\omega(\mathcal{F})} \tilde{\varphi} \tilde{\mathfrak{D}} \left((\tilde{\mathfrak{I}} \bar{m}) (\tilde{\mathfrak{F}} \tilde{\varphi}) \right) = \sum_{\mathcal{G}} (\tilde{\mathfrak{E}} \tilde{\varphi}) (\tilde{\mathfrak{I}} \bar{m}) (\tilde{\mathfrak{F}} \tilde{\varphi}), \quad (\text{C.5})$$

where we have substituted eq. (48) and used that the staggered gradient operator is the skew-adjoint of the staggered divergence operator. At this point we need that the flux interpolant $\tilde{\mathfrak{F}}$ is given by the LW interpolant, which reduces to the equal weight interpolant $\tilde{\mathfrak{E}}$ in the semi-discrete limit $\delta t \rightarrow 0$. This is needed because the staggered gradient $\tilde{\mathfrak{S}}$ and the interpolant $\tilde{\mathfrak{E}}$ satisfy the discrete equivalent of the following special case of the product rule

$$\varphi \frac{d}{dx} \varphi = \frac{1}{2} \frac{d}{dx} \varphi^2 \quad \xrightarrow[\text{equivalent}]{\text{discrete}} \quad (\tilde{\mathfrak{E}}\tilde{\varphi})(\tilde{\mathfrak{S}}\tilde{\varphi}) = \frac{1}{2} \tilde{\mathfrak{S}}\tilde{\varphi}^2. \quad (\text{C.6})$$

which follows from the algebraic relation (for $a, b \in \mathbb{R}$)

$$\frac{1}{2}(a+b)(b-a) = \frac{1}{2}(b^2 - a^2).$$

Substitution of eq. (C.6) into eq. (C.5) (with $\tilde{\mathfrak{F}} = \tilde{\mathfrak{E}}$) yields

$$- \sum_{\omega(\mathcal{F})} \tilde{\varphi} \tilde{\mathfrak{A}}[\tilde{m}] \tilde{\varphi} = \frac{1}{2} \sum_{\mathcal{G}} (\tilde{\mathfrak{J}}\tilde{m})(\tilde{\mathfrak{S}}\tilde{\varphi}^2) = -\frac{1}{2} \sum_{\omega(\mathcal{F})} \tilde{\varphi}^2 \tilde{\mathfrak{D}}(\tilde{\mathfrak{J}}\tilde{m}) = -\frac{1}{2} \sum_{\omega(\mathcal{F})} \tilde{\varphi}^2 \tilde{\mathfrak{A}}[\tilde{m}] 1,$$

which coincides, up to the sign, with the second term in the right-hand side of eq. (C.4). Hence when combined with eq. (C.4) this shows that kinetic energy is indeed conserved

$$\frac{1}{2} \frac{d}{dt} \sum_{\omega(\mathcal{F})} \rho \tilde{\alpha} \tilde{\varphi}^2 = 0.$$

References

- [1] Arrufat, T., Ciralessi-Esposito, M., Fuster, D., Ling, Y., Malan, L., Pal, S., Scardovelli, R., Tryggvason, G., and Zaleski, S. (2021). A mass-momentum consistent, Volume-of-Fluid method for incompressible flow on staggered grids. *Computers and Fluids*, 215:104785.
- [2] Bell, J. B., Colella, P., and Glaz, H. M. (1989). A second-order projection method for the incompressible Navier–Stokes Equations. *Journal of Computational Physics*, 283:257–283.
- [3] Chenadec, V. L. and Pitsch, H. (2013). A monotonicity preserving conservative sharp interface flow solver for high density ratio two-phase flows. *Journal of Computational Physics*, 249:185–203.
- [4] Cheny, Y. and Botella, O. (2010). The LS-STAG method: A new immersed boundary/level-set method for the computation of incompressible viscous flows in complex moving geometries with good conservation properties. *Journal of Computational Physics*, 229(4):1043–1076.
- [5] Crockett, R. K., Colella, P., and Graves, D. T. (2011). A Cartesian grid embedded boundary method for solving the Poisson and heat equations with discontinuous coefficients in three dimensions. *Journal of Computational Physics*, 230(7):2451–2469.
- [6] Desjardins, O. and Moureau, V. (2010). Methods for multiphase flows with high density ratio. *Center for Turbulence Research Proceedings of the Summer Program*, pages 313–322.
- [7] Desmons, F. and Coquerelle, M. (2021). A generalized high-order momentum preserving (HOMP) method in the one-fluid model for incompressible two phase flows with high density ratio. *Journal of Computational Physics*, 437(April).

- [8] Dröge, M. (2007). *Cartesian grid methods for turbulent flow simulation in complex geometries*. PhD thesis, University of Groningen.
- [9] Dröge, M. and Verstappen, R. (2005). A new symmetry-preserving Cartesian-grid method for computing flow past arbitrarily shaped objects. *International journal for numerical methods in fluids*, 47(8-9):979–985.
- [10] Etienne, S., Scolan, Y.-M., and Brosset, L. (2018). Numerical study of density ratio influence on global wave shapes before impact. In *ASME 2018 37th International Conference on Ocean, Offshore and Arctic Engineering (OMAE2018-78624)*.
- [11] Favrie, N., Gavriluk, S., Nkonga, B., and Saurel, R. (2014). Sharpening diffuse interfaces with compressible flow solvers. *Open Journal of Fluid Dynamics*, 04(01):44–68.
- [12] Gerrits, J. and Veldman, A. (2003). Dynamics of liquid-filled spacecraft. *Journal of Engineering Mathematics*, 45(1):21–38.
- [13] Harvie, D. J. and Fletcher, D. F. (2001). A new volume of fluid advection algorithm: the defined donating region scheme. *International Journal for Numerical Methods in Fluids*, 35(1):151–172.
- [14] Hernandez, J., Lopez, J., Gomez, P., Zanzi, C., and Faura, F. (2008). A new volume of fluid method in three dimensions - Part I: Multidimensional advection method with face-matched flux polyhedra. *International Journal for Numerical Methods in Fluids*, 58:897–921.
- [15] Hirt, C. W. and Nichols, B. D. (1981). Volume of fluid (VOF) method for the dynamics of free boundaries. *Journal of Computational Physics*, 39(1):201–225.
- [16] Ivey, C. B. and Moin, P. (2017). Conservative and bounded volume-of-fluid advection on unstructured grids. *Journal of Computational Physics*, 350:387–419.
- [17] Kleefsman, T. (2005). *Water Impact Loading on Offshore Structures*. PhD thesis, Rijksuniversiteit Groningen.
- [18] Leveque, R. J. (1996). High-resolution conservative algorithms for advection in incompressible flow. *SIAM Journal on Numerical Analysis*, 33(2):627–665.
- [19] Leveque, R. J. (2004). *Finite-Volume Methods for Hyperbolic Problems*. Cambridge University Press.
- [20] Lipnikov, K., Manzini, G., and Shashkov, M. (2014). Mimetic finite difference method. *Journal of Computational Physics*, 257:1163–1227.
- [21] Liu, X.-d., Fedkiw, R. P., and Kang, M. (2000). A boundary condition capturing method for Poisson’s equation on irregular domains. *Journal of Computational Physics*, 160:151–178.
- [22] Lopez, J., Hernandez, J., Gomez, P., and Faura, F. (2004). A volume of fluid method based on multidimensional advection and spline interface reconstruction. *Journal of Computational Physics*, 195:718–742.
- [23] López, J., Hernández, J., Gómez, P., Zanzi, C., and Zamora, R. (2020). VOFTools 5: An extension to non-convex geometries of calculation tools for volume of fluid methods. *Computer Physics Communications*, 252:107277.

- [24] Owkes, M. and Desjardins, O. (2014). A computational framework for conservative, three-dimensional, unsplit, geometric transport with application to the volume-of-fluid (VOF) method. *Journal of Computational Physics*, 270:587–612.
- [25] Owkes, M. and Desjardins, O. (2017). A mass and momentum conserving unsplit semi-Lagrangian framework for simulating multiphase flows. *Journal of Computational Physics*, 332:21–46.
- [26] Pilliod, J. E. and Puckett, E. G. (2004). Second-order accurate volume-of-fluid algorithms for tracking material interfaces. *Journal of Computational Physics*, 199(2):465–502.
- [27] Preisig, M. and Zimmermann, T. (2010). Two-phase free-surface fluid dynamics on moving domains. *Journal of Computational Physics*, 229(7):2740–2758.
- [28] Puckett, E. G., Almgren, A. S., Bell, J. B., Marcus, D. L., and Rider, W. J. (1997). A high-order projection method for tracking fluid interfaces in variable density incompressible flows. *Journal of Computational Physics*, 130(2):269–282.
- [29] Rider, W. J. and Kothe, D. B. (1997). Reconstructing volume tracking. *Journal of Computational Physics*, 141:112–152.
- [30] Rudman, M. (1998). A volume-tracking method for incompressible multifluid flows with large density variations. *Numerical Methods in Fluids*, 378(6):357–378.
- [31] Saurel, R. and Abgrall, R. (1999). A multiphase Godunov method for compressible multifluid and multiphase flows. *Journal of Computational Physics*, 150(2):425–467.
- [32] Scardovelli, R. and Zaleski, S. (2000). Analytical relations connecting linear interfaces and volume fractions in rectangular grids. *Journal of Computational Physics*, 164:228–237.
- [33] Sweby, P. (1984). High resolution schemes using flux limiters for hyperbolic conservation laws. *SIAM Journal on Numerical Analysis*, 21(5):995–1011.
- [34] Tryggvason, G., Scardovelli, R., and Zaleski, S. (2011). *Direct numerical simulations of gas-liquid multiphase flows*. Cambridge University Press.
- [35] Van der Plas, P. (2017). *Local Grid Refinement for Free-Surface Flow Simulations*. PhD thesis, Rijksuniversiteit Groningen.
- [36] Veldman, A. E. P. (2019). A general condition for kinetic-energy preserving discretization of flow transport equations. *Journal of Computational Physics*, 398:108894.
- [37] Veldman, A. E. P., Gerrits, J., Luppens, R., Helder, J. A., and Vreeburg, J. P. B. (2007). The numerical simulation of liquid sloshing on board spacecraft. *Journal of Computational Physics*, 224(1):82–99.
- [38] Verstappen, R. and Veldman, A. E. P. (2003). Symmetry-preserving discretization of turbulent flow. *Journal of Computational Physics*, 187(1):343–368.
- [39] Vukčević, V., Jasak, H., and Gatin, I. (2017). Implementation of the ghost fluid method for free surface flows in polyhedral finite volume framework. *Computers and Fluids*, 153:1–19.
- [40] Weymouth, G. D. and Yue, D. K. (2010). Conservative Volume-of-Fluid method for free-surface simulations on Cartesian-grids. *Journal of Computational Physics*, 229(8):2853–2865.

- [41] Youngs, D. L. (1982). Time-dependent multi-material flow with large fluid distortion. In *Numerical Methods in Fluid Dynamics*. Academic Press.
- [42] Zhang, Q. and Ding, L. (2019). Lagrangian flux calculation through a fixed planar curve for scalar conservation laws. *SIAM Journal on Scientific Computing*, 41(6):A3596–A3623.
- [43] Zuzio, D., Orazzo, A., Estivalèzes, J. L., and Lagrange, I. (2020). A new efficient momentum preserving Level-Set/VOF method for high density and momentum ratio incompressible two-phase flows. *Journal of Computational Physics*, 410:109342.